



Cite this: *RSC Adv.*, 2023, **13**, 31273

Advances in solar energy harvesting integrated by van der Waals graphene heterojunctions

Top Khac Le, ^{†ab} The-Hung Mai, ^{†c} Muhammad Aamir Iqbal, ^d Dimitra Vernardou, ^e Van-Duong Dao, ^f Vinoth Kumar Ponnusamy, ^{*ghi} Chandra Sekhar Rout ^{ji} and Phuong V. Pham ^{*c}

Graphene has garnered increasing attention for solar energy harvesting owing to its unique features. However, limitations hinder its widespread adoption in solar energy harvesting, comprising the band gapless in the molecular orbital of graphene lattice, its vulnerability to oxidation in oxidative environments, and specific toxic properties that require careful consideration during development. Beyond current challenges, researchers have explored doping graphene with ionic liquids to raise the lifespan of solar cells (SCs). Additionally, they have paid attention to optimizing graphene/Si Schottky junction or Schottky barrier SCs by enhancing the conductivity and work function of graphene, improving silicon's reflectivity, and addressing passivation issues at the surface/interface of graphene/Si, resulting in significant advancements in their power conversion efficiency. Increasing the functional area of graphene-based SCs and designing efficient grid electrodes are also crucial for enhancing carrier collection efficiency. Flaws and contaminants present at the interface between graphene and silicon pose significant challenges. Despite the progress of graphene/Si-based photovoltaic cells still needs to catch up to the efficiency achieved by commercially available Si p–n junction SCs. The low Schottky barrier height, design-related challenges associated with transfer techniques, and high lateral resistivity of graphene contribute to this performance gap. To maximize the effectiveness and robustness of graphene/Si-based photovoltaic cells, appropriate interlayers have been utilized to tune the interface and modulate graphene's functionality. This mini-review will address ongoing research and development endeavors using van der Waals graphene heterojunctions, aiming to overcome the existing limitations and unlock graphene's full potential in solar energy harvesting and smart storage systems.

Received 4th September 2023
 Accepted 6th October 2023

DOI: 10.1039/d3ra06016k
rsc.li/rsc-advances



^aFaculty of Materials Science and Technology, University of Science, Ho Chi Minh City 700000, Vietnam

^bVietnam National University, Ho Chi Minh City 700000, Vietnam

^cDepartment of Physics, National Sun Yat-sen University, Kaohsiung 80424, Taiwan.
 E-mail: phuongpham@mail.nsysu.edu.tw

^dSchool of Materials Science and Engineering, Zhejiang University, Hangzhou 310027, China

^eDepartment of Electrical and Computer Engineering, School of Engineering, Hellenic Mediterranean University, Heraklion 71410, Greece

^fFaculty of Biotechnology, Chemistry, and Environmental Engineering, Phenikaa University, Hanoi 100000, Vietnam

^gDepartment of Medicinal and Applied Chemistry and Research Center for Precision Environmental Medicine, Kaohsiung Medical University, Kaohsiung 807, Taiwan.
 E-mail: kumar@kmu.edu.tw

^hDepartment of Medical Research, Kaohsiung Medical University Hospital, Kaohsiung 807, Taiwan

ⁱDepartment of Chemistry, National Sun Yat-sen University, Kaohsiung 80424, Taiwan

^jCentre for Nano and Material Sciences, Jain University, Bangalore 562112, India.
 E-mail: r.chandrasekhar@jainuniversity.ac.in

[†] These authors contributed equally to this work.

1. Introduction

Climate change mitigation, increasing demand for energy, and global energy transformation are driving forces toward an array of alternative renewable energy sources other than traditional fossil fuels. Despite numerous availability sustainable energy resources, solar energy is recognized as a representative environmentally-friendly energy source with inexhaustible and fewer limitations compared to other alternatives such as wind and hydro. This has caught the attention of both scientific and industrial community's bio-friendly and renewable nature to the identification of solar energy harvesting devices as the holistic and cleanest energy sources to explore in serious global energy crisis terms (Fig. 1). In this context, the quest for innovative and sustainable energy in taking advantage of existing traditional carbon systems has been the center for advancing solar cells (SCs) and photovoltaic (PV) technologies to address the ever-increasing need for environmentally friendly and emission-free energy.

However, the classification of SCs is organized into three categories of generations.¹ The first category comprises single-

Solar Energy Harvesting

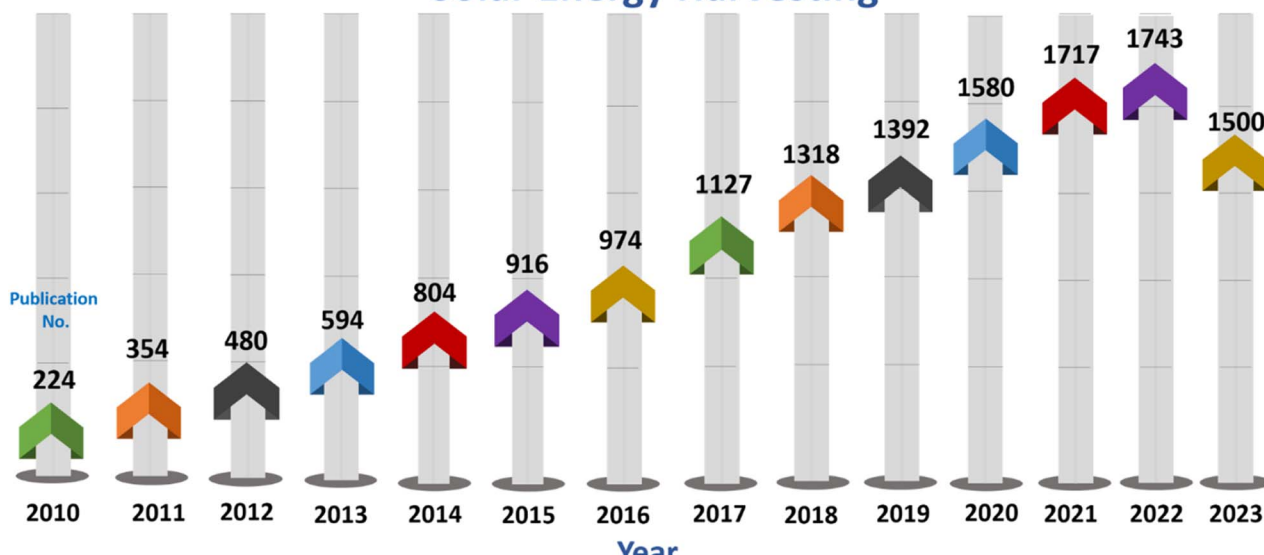


Fig. 1 The publication numbers of "solar energy harvesting" in terms of 2010–2023 (WOS Source).

and poly-crystalline Si, which boast the highest efficiency level (26.6%).² The next classification refers to SCs that employ a cadmium telluride thin film (CdTe) and copper indium gallium selenide (CIGS) with the highest reported performance (23.35%).³ Including various sub-categories, the third category involves the SCs based on newly found materials and has been widely explored to enhance the efficiency of SCs.⁴ In addition, SCs using 2D materials *e.g.*, MoS₂, WSe₂, and graphene are classified in a diverse category.^{5–9} Currently, research and development (R&D) as along with commercialization activities of Si-based SCs are mostly directed in enhancing the power conversion efficiency (PCE) while reducing manufacturing expenses.¹⁰ Interestingly, graphene has been found to be a promising candidate to revolutionize the SC market. Extensive studies have examined the integration of graphene into Si PV technology, motivated by the extraordinary physical properties of graphene. These attributes encompass exceptional electrical conductivity, carrier mobility, thermal conductivity, mechanical flexibility, stability, and dominant transmittance (97.7% monolayer graphene in visible region).^{11–13} Thus, the R&D efforts focused on incorporating graphene into devices used for SCs have rapidly progressed, resulting in high PCEs exceeding 15% in copious distinguished applications. Several works associated with incorporating of graphene into PVs for numerous vital roles, such as the active layer and electrode, have been reported.^{14–16}

One crucial challenge in creating high-performance SCs for energy harvesting and practical implementations is the efficient generation/separation of paired electron–hole from photo-induced processes, followed by the effective transfer of these separated charge carriers to the electrodes. In this context, graphene revealed significant improvement. Consequently, research has been performed to explore and evaluate the graphene/Si Schottky junction (G/S-SJ) device for various

applications utilizing the internal photoemission process. Hence, SCs that utilize a SJ, with graphene acting as a metal and Si as a semiconductor, have been duly recognized as a suitable example of Schottky junction devices (SJDs).¹⁷

In this review, the emergence of G/S SB-SCs and PVs concerns are exhibited in relation to the extensive endeavors to enhance the performance of low-cost SCs. The charge transport mechanism in G/S SB-SCs is elucidated, along with several approaches that facilitate the optimization of such devices for PCE to explore the further mechanism principle of the hetero-structured devices. Additionally, the difficulties and potential opportunities associated with G/Si SB-SCs in the field of PV technology are discussed, with the aim of paving the way for the design of next-generation solar energy harvesting systems.

2. Emergence of graphene/Si in solar cells and photovoltaics

Among the different 2D materials, graphene, a well-known carbon allotropes, was first fabricated in 2004 by Novoselov *et al.* using mechanical exfoliation of graphite.¹¹ It comprises a monolayer of carbon atoms arranged in a hexagon network.^{7,18–42} Thus, graphene has been shown as a greatly promising material for future optoelectronic devices due to its remarkable features, including high mobility reaching up to 10^4 cm² V^{−1} s^{−1} at ambient temperature, exceptional thermal and electric conductivities, and ballistic transport.^{12,43} Also, in the broad spectra range of visible and near-infrared (NIR), the transmittance of single layer graphene can reach 97.7%, and only 2.3% of the light intensity can be absorbed.^{44,45} As a result of its thin structure, graphene enables a substantial section of sunlight to permeate through it.⁴⁶ The exceptional optical and electronic features of graphene have positioned it as a highly favorable prospect for the design and production of SCs.



Graphene has a dual role, functioning as both a target electrode in Schottky junction or Schottky barrier solar cells (SB-SCs) and an active layer. Additionally, it possesses flexibility and is widely abundant on a global scale. This has inspired significant interest in substituting FTO and ITO substrates⁴⁷ for producing high-performance and low-cost solar panels, including graphene/Si solar cells (G/S-SCs).⁴⁸ Additionally, the capacity to adjust the ϕ_{wf} of graphene enables it to function as either p- or n-type electrodes.⁴⁹ Additionally, graphene typically exhibits excellent environment stability,⁵⁰ exceptional mechanical strength,⁵¹ and high crystalline quality during upscale compared with other 2D materials *e.g.*, MoS₂, WS₂, WSe₂, *etc.*⁵² These characteristics render graphene-based SCs advantageous over the first generation of PVs. As a result, there has been a substantial increase in the abundance of work conducted on G/S SCs recently.⁵³⁻⁵⁷

Owing to its physical/chemical/mechanical features, graphene-based heterojunction SCs exhibited an good efficiency (18.5%) when combined with GaAs structure.⁵⁸ After achieving positive results in research and development trials, a feasible manufacturing process for small-scale commercial production of thin-film and dye-sensitized photo-supercapacitors using graphene has been effectively developed and implemented.⁵⁹⁻⁶¹ However, large-scale manufacturing of these SC types remains challenging to date. SB-SCs, which are made using the method of direct deposition of a transparency electrode or thin film of metal on a moderately doped semiconductor wafer, have gained significant attention in PVs.⁶² They have advantages over traditional p-n junction SCs in terms of being inexpensive and simple to manufacture.⁶³ Nevertheless, conventional SB-SCs require a thick metal layer that hinders solar radiation absorption. Thus, ITO has been explored as an alternative, but its limited resources and fragile nature limit its application in flexible devices. To overcome these challenges, graphene sheets have been successfully employed in SB-SCs, permitting the production of cost-effective, flexible solar panels with excellent environmental stability, eco-friendliness, and efficiency exceeding 10%. The demand for flexible SCs in various applications including wearable/implantable microsystems and wireless sensor networks for IoT, makes G/Si SB-SCs highly attractive for the PVs market.

Recently, the vehement efforts have been proceeded to develop new-generation G/Si SB-SCs, with a signify attention on chemical doping techniques to achieve high Schottky barrier height and efficiency. However, the chemical-doped G/Si SCs often exhibit rapid degradation due to the oxidative nature of the dopants. An alternative promising strategy is being explored to develop the chemical-doping-free G/Si SCs, which exhibit stability over several months. Regrettably, the effectiveness of these SCs is limited due to the high electrical resistance of graphene films and the low Schottky barrier of the G/Si heterojunction. Recently researches show that the PCE of G/Si SCs has been enhanced by doping technique with PbS quantum dots⁶⁴ and electrical-field doping with a liquid gate circuit.⁶⁵ Chemical doping into the graphene can generate more acceptor carriers and improve conductivity. However, they have limitations including significant light loss and the instability of the

integrated liquid medium that prevent them from being used in practice.⁶⁶

On the other hand, doping effects caused by solid interactions have been documented in graphene-assisted heterojunctions *e.g.*, MoF₆/graphene^{67,68} and MoO₃/graphene.⁶⁹ This advancement's lack of chemical reactions offers a promising approach for achieving steady graphene doping. From this perspective, a study was conducted to explore the interactions in graphene/fluorographene heterostructures, targeting to improve the output of G/Si SCs. Interestingly, fluorographene is a novel derivative of graphene that features dipoles created by C-F bonds in graphite, making it one of the thinnest known insulators. It is made by revealing graphene to fluoride gases, and its electrical features are adjusted *via* its C/F ratio.⁶⁸ Simulated studies have demonstrated the interactions between graphene with other 2D materials (graphene and MoS₂). Notably, the F atoms present in fluorographene function as receptors of electrons, leading to the transfer of charge-coupled 2D elements onto fluorographene and potentially causing p-type doping. Density functional theory (DFT) was employed to examine the optical characteristics of graphene hexagonal boron nitride (h-BN) and fluorographene.⁷⁰ Fluorographene exhibits exceptional capability in decoupling graphene from the substrate. These distinctive properties make fluorographene an attractive option for optimizing G/Si SCs.

The pioneering study by Zhu *et al.* in 2010 explored the feasibility of G/n-Si SB-SCs achieving an efficiency of 1.65%.⁴⁸ G/Si SB-SCs hold promise for effectively separating charge carriers due to their substantial built-in potential. Graphene holds a key role for the efficiency of these SCs because it acts as both active layer and transparent electrode.^{71,72} This requires the graphene to exhibit more physical properties such as good photo-generated charge carriers, high electron mobiles safely electron transport. In less than 10 years, G/Si SB-SCs achieved up to 15% efficiency due to the 100 times greater than (approximately $2.5 \times 10^5 \text{ cm}^2 \text{ V}^{-1} \text{ s}^{-1}$) of electron mobility comparing Si substrate.⁷³ Graphene, being a zero-band-gap semiconductor, exhibits the remarkable ability to absorb light across a broad spectrum. Moreover, electrons within graphene can traverse several micrometers without scattering, showcasing its exceptional transport characteristics.⁷⁴ SCs using graphene such as hole transporter based on G/Si structure were first created by depositing a graphene thin film on Si surface.⁴⁸ However, the graphene layer exhibited higher sheet resistance (a few k Ω), negatively affecting its conductivity. Consequently, it impeded the flow of photo-generated current in G/Si SCs, leading to an extraordinary reduction in their PCE. Initially, researchers explored the chemical doping on a top graphene surface, which involved the introduction of a p-type dopant into the graphene material. However, HNO₃ and bis-(trifluoromethane sulfonyl) amide (TFSA) are the most widely utilized dopants in G/Si SCs.^{75,76} By introducing a TFSA layer, the highest reported increase in efficiency (1.9% to 8.6%) of G/Si SCs with the use of doping was achieved. Also, several other dopants, such as boron doping⁷⁷ and doping with chemicals such as SOCl₂, HNO₃, HCl, and H₂O₂ were introduced by various research groups.^{75,78} Coating the top surface of graphene with a dopant proved



highly effective in reducing its resistance. However, despite the benefits of chemical doping, a significant limitation is its unsteadiness in the atmospheric media, leading to surface deterioration and eventually restoring the cell's efficiency to its initial value. For this reason, graphene oxide (GO) and Pt nanoparticles (NPs) have been recognized as suitable dopants for the top surface of G/Si SCs.^{79,80} In G/Si SCs, a transparent MoO₃/Ag/MoO₃ heterojunction layer over graphene was applied, resulting in an increased ϕ_{wf} , reduced series resistance, and improved efficiency (0.86 to 3.5%) of graphene.⁶⁹ Bhopal *et al.*⁸¹ reported an increase in efficiency from 4.3 to 5.01% in G/Si SCs using an Ag/Ni electrode to decrease the contact resistivity. NiO-induced doping in G/Si SCs was employed to lower the series resistance, enhance the SJ quality as well as improve cell robustness.⁸² In particular, effect contact of metallization front electrodes provides a direct electrical contact between graphene layer and the Si substrate. This low-resistance contact improves charge carrier extraction and reduces series resistance, leading to enhanced solar cells performance. Moreover, the process of depositing a metal layer onto the front surface of solar cells is well-established and relatively straightforward. Common deposition techniques like sputtering or evaporation are widely used for this purpose. While the efficiency of solar cells through the using the chemical induced doping could also be improved by enhanced carrier mobility and tunable properties. NiO is a prime example for the doping method, which can significantly promote the mobility of charge carriers. Besides, NiO doping can mitigate carrier recombination at the graphene/Si interface. By reducing recombination, the efficiency of charge carrier extraction and collection increases, leading to higher overall solar cells performance. Nevertheless, the limitations of these two methods still exist, and affects to quality of energy conversion. Typically, the controllable thickness and shape of electrodes is extremely important, due to the depending on the thickness and layout of the metal front electrode, there is a possibility of shading some of the active solar cell area, which can decrease efficiency, or in the doping method, achieving uniform doping across the entire solar cells area can be challenging, and any non-uniformity might lead to performance variations. Additionally, the stability of the NiO-doped layer and its interaction with other materials need to be accessed for potential degradation over time, which could impact long-term performance of the solar cells. Therefore, choosing the appropriate method will depend on factors such as the specific cell design, the level of performance enhanced desired, fabrication complexity, material compatibility. Furthermore, ongoing research may lead to improvements and refinements in these methods over time.

3. Structure and mechanism in graphene/Si SB-SCs

Fig. 2a illustrates the structure of G/Si SCs.⁷³ The fabrication of such a device primarily relies on the method outlined by Li *et al.*⁴⁸ The process includes the application of wet transfer to move chemical vapor deposited (CVD) graphene onto the

exposed SiO₂/n-Si. This is followed by the addition of front/rear electrode deposition, establishing the graphene/n-Si heterojunction as illustrated in Fig. 2b.⁸³ SiO₂ layer was deposited on Si, and it was etched away using a buffered oxide etchant, exposing a suitable-sized Si window. Afterward, graphene is transferred to Si substrate, accompanied by undesired graphene etching. Normally, top-notch CVD produced graphene is employed and shifted using polymethylmethacrylate (PMMA) technique. To be more precise, the graphene grown on a metal foil (Cu) is first coated with PMMA through a spin-coated process. The copper foil is then dispersed in a copper etchant solution (CuSO₄ : HCl : H₂O) for a few hours and subsequently rinsed with deionized water. Then, the PMMA-casted graphene film is relocated on Si window and metal pad. Finally, the PMMA is extracted using acetone, and the G/Si SCs are cleaned with isopropyl alcohol (IPA) to complete the fabrication process. Fig. 2c provides a schematic representation of G/Si SB-SCs based on heterojunction structure using various interfacial layers, doping, and anti-reflection coatings.⁸⁴ When graphene is in proximity to Si, carrier transfer occurs to align the Fermi levels (E_F). Electrons originating from n-type Si migrate to graphene, generating an area with reduced electron concentration. As a result, an inherent electric field forms between graphene and Si. When subjected to light, the Si substrate absorbs photons, giving rise to the generation of new electron-hole pairs. Inside the region of electron depletion, the electrons and holes generated by light are swiftly separated due to the existing electric field and are directed towards the electrodes. This process leads to the creation of a photocurrent.

4. Performance parameters

Dark current–voltage (I – V or J – V) of G/Si SJ was described by eqn (1).

$$J = J_0 \left[\exp\left(\frac{qV}{\eta k_B T}\right) - 1 \right] \quad (1)$$

where J_0 and J are the saturation current density and current density, respectively. q and k_B are the elementary charges and the Boltzmann constant of 1.6×10^{-19} C and 1.38×10^{-23} J K⁻¹, respectively. V , T , and η are the applied voltage, the absolute temperature in Kelvin, and the ideality factor, respectively. The ideality factor serves as a measure of the G/Si junction's quality and reflects the recombination of carriers at the interface. An ideality factor of 1 signifies an ideal junction. However, the ideality factor observed experimentally varies in a wide range ($0.2 \leq \eta \leq 1$). For the ideal junction, where the minority carrier recombination in the quasi-neutral area's controls recombination largely, n is equal to 1. However, the n can be 2 or greater if other recombination mechanisms occur. eqn (2) provides the representation for the reverse saturation current (J_0).

$$J_0 = A^* T^2 \exp\left(\frac{-q\phi_{\text{SBH}}}{k_B T}\right) \quad (2)$$

where A^* is the effective Richardson constant ($252 \text{ A cm}^{-2} \text{ K}^{-2}$ for n-Si and $32 \text{ A cm}^{-2} \text{ K}^{-2}$ for p-Si), and ϕ_{SBH} is the Schottky barrier height. The Schottky barrier arises when the height ϕ_{SBH}



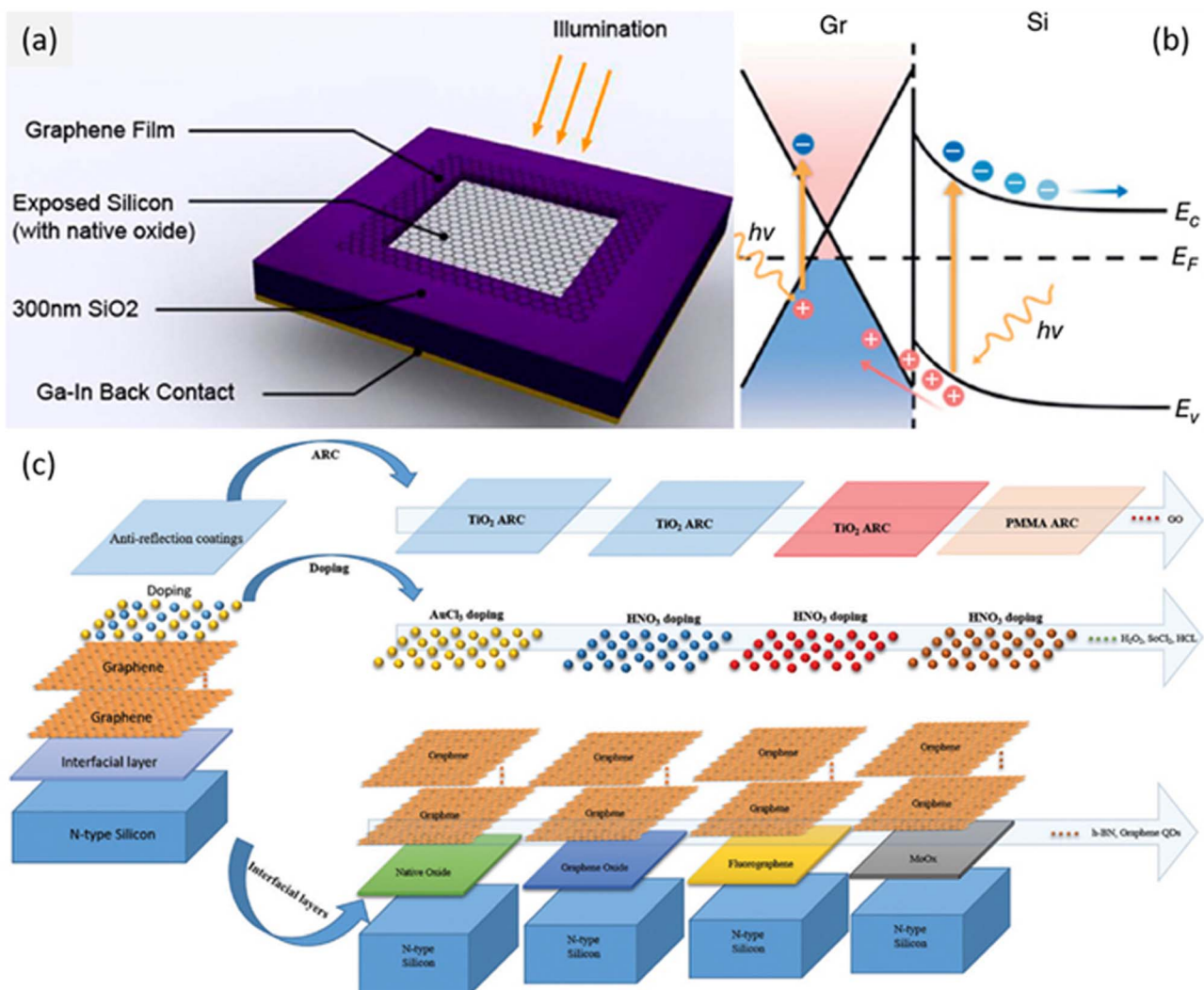


Fig. 2 (a) Design of G/n-Si SC, a layer of graphene was applied onto SiO₂/Si substrate, forming a junction. (a) has been reproduced from ref. 73 with permission from American Chemical Society. (b) Energy band diagram in G/n-Si SB-SCs and the displacement of electron–hole pairs. (b) has been reproduced from ref. 83 with permission from Wiley-VCH. (c) A visual representation depicting the uncomplicated creation of a G/Si SB-SCs through a heterojunction structure is shown. This process involves three key factors: interfacial layer, chemical doping, and ARC coating. These factors collectively contribute to improving efficiency and prolonging the durability of G/Si SCs. (c) reproduced from ref. 84 with permission from Royal Society of Chemistry.

$= \phi_{\text{metal}} - \chi_{\text{Si}}$ is established as work function of a metal (ϕ_{metal}) higher than electron affinity of the Si (χ_{Si}). This barrier effectively hinders the recombination of electrons and holes, thanks to the presence of a substantial built-in field. Upon being subjected to light radiation, electron–hole pairs are produced as a result of interactions involving both the graphene layer and the underlying bulk Si. The built-in potential (V_0) segregates these pairs, directing electrons towards n-Si and holes towards graphene. Ultimately, these charges are transported to their respective electrodes for collection.

Electron/holes at regions of G/Si junction as light illuminated will generate the photovoltage (V) and it reaches maximum value in open-circuit voltage (V_{OC}). As SC short-circuited, photogenerated carriers flow through the external circuit, resulting in a maximum current called I_{SC} . Nevertheless, in practical use, SCs function within a range that lies between

a short-circuit condition and an open-circuit condition. Due to the rectifying characteristics and non-linear voltage-current behavior of the G/Si junction, a maximum output power (P_{max}) can be achieved.

PCE of the G/Si SCs quantifies the extent to which sunlight energy is changed into electricity. It can be conveyed using eqn (3).

$$\text{PCE} = \frac{V_{\text{OC}} \times I_{\text{SC}} \times \text{FF}}{P_{\text{in}}} \quad (3)$$

where P_{in} is the incident power of light. Fill factor (FF) of a SC is defined as the ratio of P_{max} and the product of V_{OC} and I_{SC} and cab expressed as eqn (4).

$$\text{FF} = \frac{P_{\text{max}}}{V_{\text{OC}} \times I_{\text{SC}}} \quad (4)$$

External quantum efficiency (EQE) is characterized as the ratio of charge carriers to incident photons of a specific energy, and its determination can be achieved through the utilization of eqn (5).

$$\text{EQE} = \frac{I_{\text{ph}} h \nu}{q P_{\text{in}}} \quad (5)$$

Here I_{ph} represents the photocurrent, q symbolizes the elementary charge, P_{in} stands for the incoming solar power, h denotes the Planck constant, and ν corresponds to the frequency of the incoming photons.

Internal quantum efficiency (IQE) refers to the count of charge carriers for each absorbed photon within the SC. IQE is evaluated by subtracting the photons lost due to reflection and transmission from the EQE. This connection can be mathematically represented using eqn (6).

$$\text{IQE} = \frac{\text{EQE}}{1 - R - T} \quad (6)$$

where R is the reflection and T is the transmission of SCs. J_{SC} , V_{OC} , FF, EQE, and IQE are parameters to evaluate the PCE of SCs. With these parameters, we can engage in a quantitative analysis of the efficiency of G/Si SCs.

5. Theoretical efficiency limits of graphene/Si SCs

According to Shockley–Queisser (SQ) model, the PCE of SCs depends on the band gap of the active semiconductor layer. Auger recombination is also considered in reassessing the efficiency limits, resulting in the highest theoretical values for V_{OC} , J_{SC} , FF, and PCE. Other parameters such series resistance (R_s) and shunt resistance (R_{SH}) strongly affects the final current of SCs as contact with other devices. The current–voltage characteristics of SCs are described by eqn (7) and (8), representing the scenarios excluding extraneous resistances and considering both R_s and R_{SH} , respectively. In this context, R_s and R_{SH} will be treated as a constant in the simplicity of SQ model for simplicity of mathematical treatment.

$$J = J_{\text{ph}} - J_0 \left[\exp \left(\frac{qV}{\eta k_B T} \right) - 1 \right] \approx J_{\text{ph}} - J_0 \exp \left(\frac{qV}{\eta k_B T} \right) \quad (7)$$

$$J = J_{\text{ph}} - J_0 \left[\exp \left(\frac{q(V + IR_s)}{\eta k_B T} \right) \right] - \frac{V + IR_s}{R_{\text{SH}}} \quad (8)$$

where, J stands for the current density at the G/Si interface, J_0 represents the density of reverse saturation current density, J_{ph} indicate photocurrent density, V denotes the applied voltage, T represents the absolute temperature and η signifies the ideality factor.

Fig. 3a and b displays the J – V curves of G/Si SCs for varying R_s and R_{SH} values, respectively.⁸³ It is evident that the FF of the SCs exhibits a significant relationship with sheet resistance of graphene. Reducing the sheet resistance leads to increased FF, indicating that improving graphene's sheet resistance can be accomplished by focusing on high-quality growth, precise transfer, and controlled doping technique. The impact of shunt

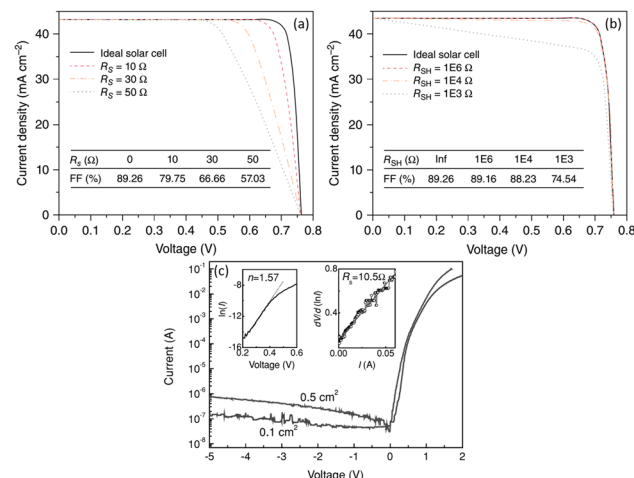


Fig. 3 Voltage–current characteristics and FF of a theoretical G/Si SCs with various (a) series resistance, (b) sheet resistance. (a) and (b) have been reproduced from ref. 83 with permission from Wiley–VCH. Experimental G/Si SCs with (c) series resistance and sheet resistance, which is estimated from the reverse bias I – V sweep. (c) has been reproduced from ref. 48 with permission from Wiley–VCH.

resistance transforms into relevance only when the resistance decreases below 10 k Ω . Otherwise, it has minimal to minimal results on the efficiency of G/Si SCs regardless of any variation in resistance. Given the provided experimental values for parasitic resistance ($R_s = 10.5 \Omega$, $R_{\text{sh}} = 45 \text{ M}\Omega$), it can be concluded that the impact of series resistance on efficiency is significantly more detrimental (Fig. 3c).

6. Strategies for enhancing efficiency of graphene/Si SCs

The SC efficiency was affected by absorption, hole–electron pair generation, diffusion of electron, lifetime of electron, etc. Recently research show strategies to enhance the performance of G/Si SCs such as doping in graphene material, and light trapping in Si substrate.

6.1. Influence of dopants

Graphene serves as both transparent conductor and junction layer in G/Si SCs. As a transparent conductor, graphene should exhibit high electrical conductivity and transparency. Fig. 3a demonstrates the significant impact of graphene's sheet resistance on the performance of G/Si SCs. Studies show that the resistance of graphene was reduced by strategies such as doping, multilayer combination, and surface modification. Nevertheless, the process is complicated due to a trade-off between transparency and sheet resistance. Adding a layer of graphene leads to a decrease in transparency of approximately 2.2–2.3%.⁷⁸ Therefore, optimizing both transparency and sheet resistance is important for accomplishing higher efficiency G/Si SCs. For instance, the resistance of stacking graphene layers and sheet resistance of bi- and tri-layer graphene decreased from 980 $\Omega \text{ sq}^{-1}$ (single layer graphene) to 540 and 350 $\Omega \text{ sq}^{-1}$



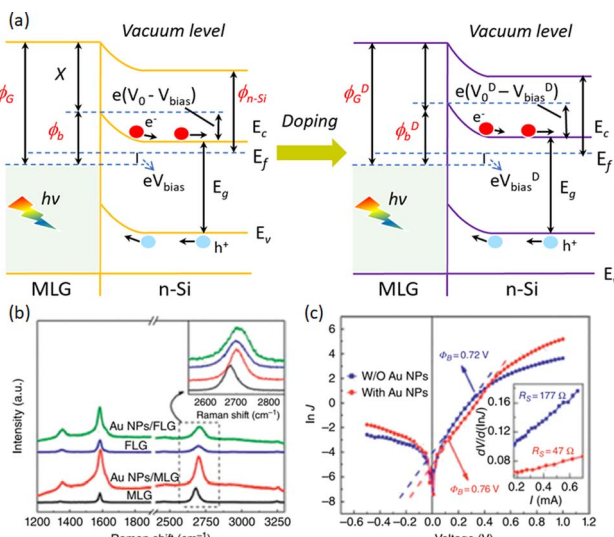


Fig. 4 (a) The diagram of band structure and ϕ_{wf} of the MLG/Si interface prior to and following the doping process. (b) Raman spectroscopy results showing the spectra of MLG and FLG with and without the presence of Au NPs. (c) Dark J-V curves of the FLG/Si SCs with and without Au NPs. The inset presents the graphs of $dV/d(\ln J)$ versus I , enabling the determination of the series resistance R_s of cells. (b)–(d) have been reproduced from ref. 89 with permission from American Institute of Physics.

while the transparency decreased from 97.6% (single layer graphene) to 92.9%.⁷⁸ The good conductivity of eight-layered graphene of $180 \Omega \text{ sq}^{-1}$ leads to the decrease in transparency from 90.8% (four-layered) to 83%.⁷⁸ These results clearly illustrate the correlation between transparency and sheet resistance. However, there are some advantageous outcomes, stacking individual MLG is not a simple task. The stacking of layers one by one is a time-intensive procedure that lacks scalability and introduces polymeric and environmental contaminations during the transfer and stacking stages (Fig. 4).

Aside from increasing the number of layers, doping has been established as an effective method for reducing the sheet resistance of graphene. Different doping approaches using chemical doping have been successfully utilized. Heteroatom doping involves the substitution or bonding of atoms like oxygen, boron, nitrogen, phosphorus, and sulfur, with carbon atoms in the graphene lattice. Nevertheless, dopants are chosen over heteroatom doping for application in G/Si SCs. Amongst different dopants, HNO_3 , SoCl_2 , and AuCl_3 have shown promising results. Cui *et al.* found that SoCl_2 is the most effective dopant to improve the PCE of SCs to 2.3% due to decreased sheet resistance from 735 to $405 \Omega \text{ sq}^{-1}$. Feng *et al.* with demonstrated a reduction in series resistance (R_s) of the SCs from $6.11 \Omega \text{ cm}^2$ to $4.07 \Omega \text{ cm}^2$ and an improvement in PCE from 2.9% to 4.35% after immersing the device in HNO_3 , along with V_{OC} , J_{SC} , FF enhancement to 495 mV, 17.22 mA cm^{-2} and 51%, respectively.^{72,85} Although chemical doping has shown promising results in reducing graphene resistance and SC efficiency, there is concern regarding the durability of the covalent functionalization of graphene. Degradation of the

functionalization caused by the ambient air can result in a significant decrease in PV enhancement by up to 50%. However, doping by gold chloride (AuCl_3) has demonstrated better environmental stability than other reported methods.⁸⁶ The reduction of Au^{3+} to Au NPs by transferring charges from graphene results in p-doping of graphene, leading to substantial enhancements in conductivity. The sheet resistance by AuCl_3 -doped MLG results in reducing sheet resistance and enhancing efficiency.^{73,87}

In addition, doping with organic compounds can also improve the physical properties of graphene.^{90,91} For example, doping with trifluoromethanesulfonic amide (TFSA) resulted in an increase in the PCE of the G/Si device was increased 1.9% to 8.6%, an increase in the J_{SC} from 14.2 to 25.3 mA cm^{-2} , and an increase in the V_{OC} from 0.43 to 0.54 V , for doped and un-doped graphene, respectively.⁷⁶ When TFSA is functionalized on monolayer graphene, it has been observed that the resistance decreases from 1200 to $300 \Omega \text{ cm}^{-2}$ without notable impact on transmittance. Most of these dopant's p-dope the graphene, leading to a decrease in the sheet resistance of graphene by shifting the graphene Fermi level downward or increasing the ϕ_{wf} . Since graphene also behaves as a junction layer, the increase in the ϕ_{wf} has additional implications at the interface. The enhanced graphene ϕ_{wf} leads to an elevated SBH, thereby establishing a more robust built-in electric field and more efficient separation of carriers. As depicted in Fig. 4a, the rise in V_{OC} following the doping process enhances the built-in potential V_o and the barrier height (ϕ_b). This adjustment aligns with the variance of the work function of MLG (ϕ_G) and the electron affinity of Si (χ).⁸⁸ Chemical doping raises ϕ_G , promoting enhanced charge transfer and collection at the interface. Consequently, the enhancement brought about by doping in the G/Si SCs combines improvements in graphene sheet resistance and an elevated Schottky barrier height.

Taking into consideration the instability of chemical doping, it is not practical for the utilization of graphene/Si PV devices. Therefore, more reliable doping techniques are increasingly coveted, and researchers have recently commenced investigating alternative approaches including physical and light-induced doping. Some metals (metal's EF lower than graphene's EF) have been found to effectively p-dope graphene. The

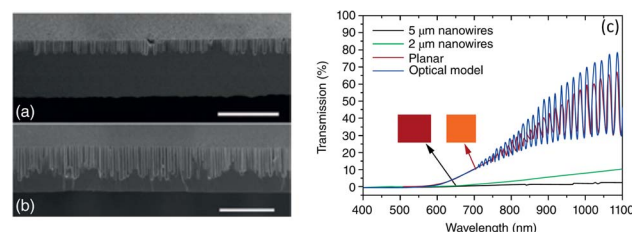


Fig. 5 Tilted cross-sectional SEM images visualizing (a) arrays of nanowires measuring $2 \mu\text{m}$ and (b) arrays of nanowires measuring $5 \mu\text{m}$. Scale bars are $10 \mu\text{m}$ for both images. In addition, (c) transmission spectra of thin Si structures are provided for the comparison: prior to etching (red), subsequent to etching into $2 \mu\text{m}$ (green), and following etching into $5 \mu\text{m}$ (black) nanowires. (a)–(c) have been reproduced from ref. 92 with permission from American Chemical Society.

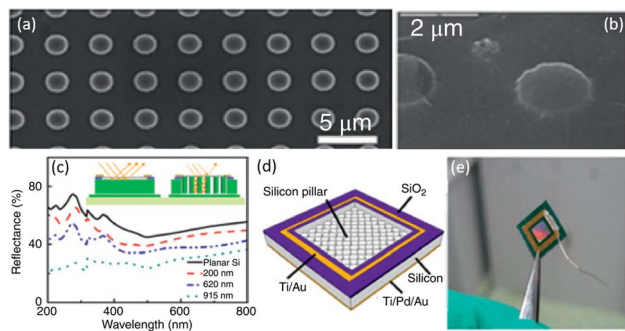


Fig. 6 SEM image of Si pillar without (a) and with coated graphene (b). (c) the reflectance spectra of Si pillars with different pillar height and planar Si substrate. Inset presents the principle of antireflective effect of Si pillar substrate. (d) Schematic presentation of a G/Si pillar SB-SCs. (e) Photograph of a G/Si pillar SC with junction area of 0.09 cm^2 . (a)–(e) have been reproduced from 72 with permission from American Institute of Physics.

doping capacity of metal NPs is determined by their ϕ_{wf} , with metals possessing higher ϕ_{wf} demonstrating more effective graphene doping. Successful p-doping is indicated by a blue shift in the 2D Raman peak upon deposition of Au NPs (Fig. 4b).⁸⁹ By optimizing the Au NPs size, the PCE of G/Si SCs was increased to 7.34%. Au/HNO₃ co-doped graphene increases the efficiency to 10.20% by achieving a raised ϕ_{wf} and improved electrical conductivity of graphene. As depicted in Fig. 4c, the reduction in the series RS of Schottky diode, attributed to the introducing of Au NPs, not only results in a heightened FF but also enhanced J_{sc} .⁸⁹ This outcome aligns with findings from previous studies on the effects of HNO₃ doping. Similarly, the work shows a high efficiency of 10.69% with Au/TFSA co-doped graphene.⁹⁰ NPs of another metal, Pt, with a high ϕ_{wf} , have also been demonstrated to enhance the PCE to 7% through the integration of physical doping using high ϕ_{wf} Pt NPs, improved absorption of SCs in the visible region due to plasmonic effect and the photo-induced doping. Approaches to providing holes

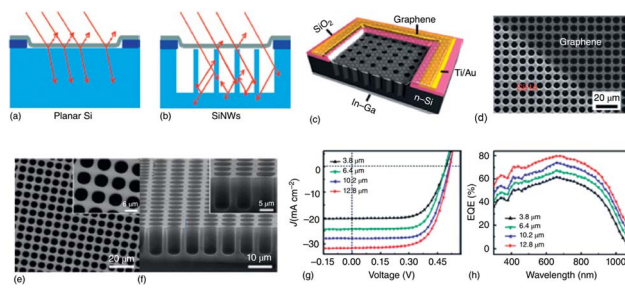


Fig. 7 (a) Schematics diagrams of G/planar Si, (b) G/Si NW junctions. (a) and (b) have been reproduced from ref. 94 with permission from American Chemical Society. (c) Schematic presentation of the G/Si HA SB-SCs, (d) top-view SEM image of the G/Si HA device. The area included by graphene films shows darker contrast in the SEM image. (e) Top-view and (f) cross-sectional view SEM images of the as-prepared SiHA. Insets present the enlarged SEM images, (g) PV characteristics, and (h) EQE spectra of the G/Si HA SB-SCs with various hole depths. (c)–(h) have been reproduced from ref. 95 with permission from Royal Society of Chemistry.

or electrons to graphene by using P3HT or TiO₂ film were used. The suitability of HUMO of P3HT and VB of Si creates favorable conditions for hole transport under light illumination, enhancing carrier concentration. On the other hand, holes were captured by the traps in TiO₂ whereas the electrons were moved to graphene.

In addition, prolong stable of SCs play a signify role. TiO_x material coated on graphene can remain or reduce the degradation of PCE of SCs. A PCE value of 12.95% was reached, with degradation of less than 10% after 1-month storage by coated TiO₂ layer.⁹¹ Efficiency levels of 8.2% and 10.5% were achieved for TiO_x/G/p-Si without PMMA and with antireflection (AR) coating of PMMA, respectively. Furthermore, no significant changes in performance were observed over a period of 10 days.⁹² GO is a multi-functional component for G/Si SCs. For example, GO layer functions as p-type dopant for graphene and also acts as an AR layer within SC. PCE of the G/GO/Si CSs maintained a consistent 10% level over a span of 20 days.⁷⁹ Using GO as a passivation layer led to a significant improvement in the lifetime of carriers.⁹³ Simultaneously, GO also functioned as a protective; however, its barrier characteristics were observed to diminish at elevated temperatures (400 °C) because of GO decomposition and alterations in its doping levels.⁹³

6.2. Influence of light trapping in silicon

The planar Si plays a significant importance for light absorption and electro/hole pairs generation. Therefore, the enhanced absorption of Si leads to an improvement in efficiency. However, planar Si exhibits high reflection. This drawback of planar Si induces the reduction efficiency of SC due to absorption losses. Nevertheless, the integration of micro/nano structures on the silicon surface can substantially enhance the light absorption capacity owing to the pronounced light-trapping phenomenon. This phenomenon effectively diminishes the sunlight reflection from the surface of the junction, resulting in enhanced charge-collection efficiency. For instance, employing patterning in the form of Si nanowires can increase the distance traveled by incident solar radiation by a factor as substantial as 73.^{92,93}

Fig. 5a and b describe the cross-section of Si nanowires of 2 μm and 5 μm .⁹² The transmittance spectra show that both Si nanowires of 2 μm and 5 μm before etching exhibit low transmittance.⁹² It is evident that correlated to planar Si, nanowires exhibit decreased transmission indicating strong light trapping. Similarly, in the case of G/Si SCs, texturing Si into structures such as pillars, nanowires, pyramids, etc. has been employed to minimize light reflection and enhance light absorption. These non-planar features redirect the incident light back into the Si rather than allowing it to transmit through the Si, leading to improved absorption through light trapping and subsequently boosting the overall PCE. Fan *et al.* fabricated Si NWs through metal-assisted etching method.⁹⁴ The G/Si NWs SJ demonstrated higher absorption contrasted to the graphene/planar Si junction leading to the enhancing efficiency of up to 2.865% because the Si NWs contribute an



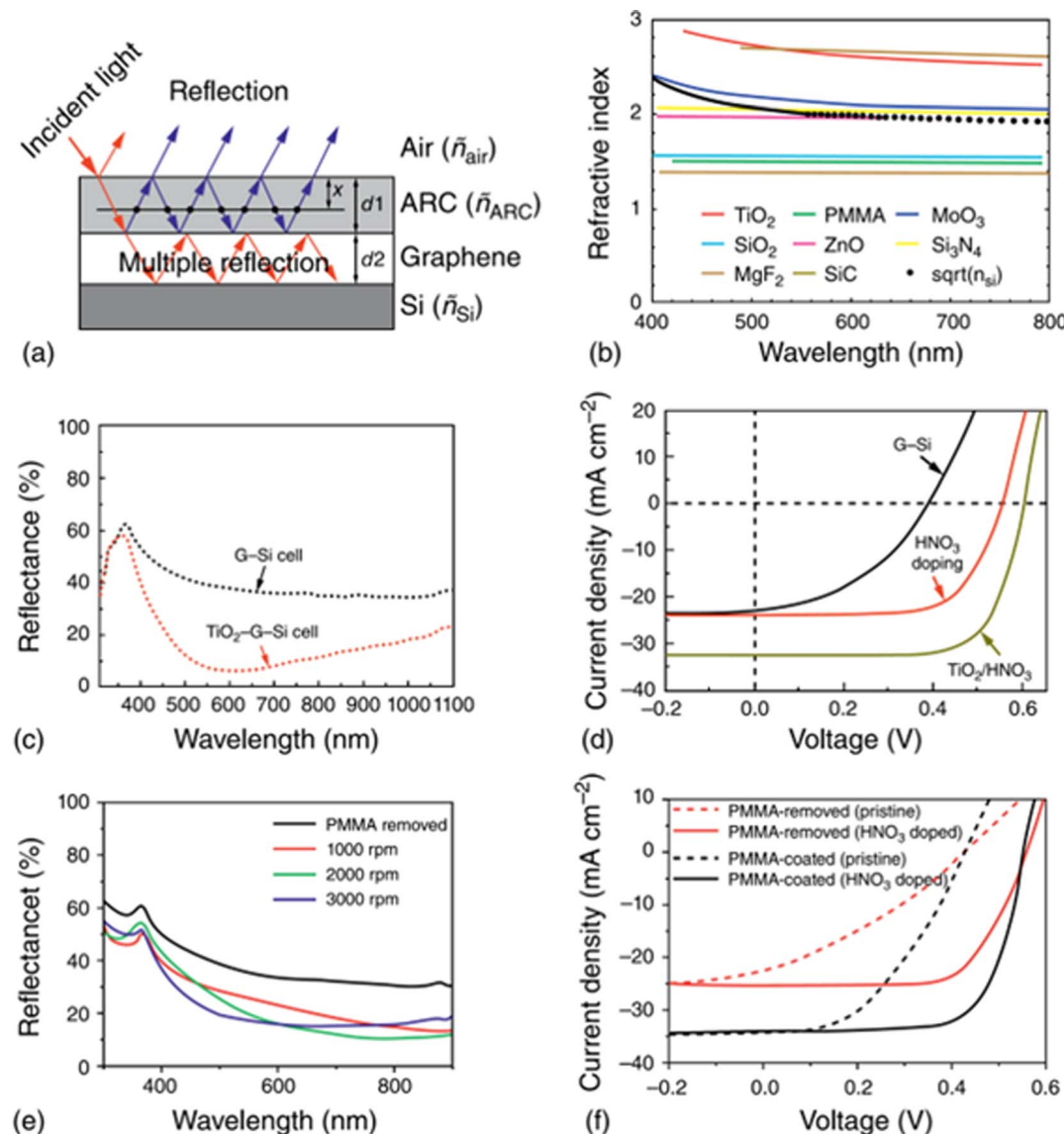


Fig. 8 (a) Patterning of the Si substrate, (b) relationship between refractive index and wavelength for certain ARC materials. (a) and (b) have been reproduced from ref. 96 with permission from Royal Society of Chemistry. (c) Light reflection spectra of a g/Si SCs prior to (black) and following (red) the application of a TiO₂ colloid coating, illustrating antireflection effect, (d) J-V characteristics of an as-deposited G/Si SCs, after HNO₃ vapor doping, and after TiO₂ coating (together with HNO₃ doping), respectively. (c) and (d) Have been reproduced from ref. 97 with permission from American Chemical Society. (e) Reflectance spectra of PMMA-extracted and PMMA-grown graphene samples on quartz slides, (f) J-V curves of PMMA-removed and PMMA-coated (2000 rpm) G/Si SCs before and after HNO₃ doping. (e) and (f) Have been reproduced from ref. 98 with permission from Royal Society of Chemistry.

immediate pathway to the overall improvement in performance due to direct and fast pathway of electron–hole collection as light trapped on the planar junction. Feng *et al.* implemented the pillar to enhance light absorption using photolithography and inductive coupled plasma (Fig. 6).⁷² The result implies that the Si pillar exhibits more absorption correlated with planar Si. The absorption intensity is strongly affected by pillar height and achieves the highest absorption with 900 nm pillar height. The PCE of G/Si pillar devices was measured to be 1.96% (which could be further enhanced to 3.55% by HNO₃ doping), surpassing that of G/planar-Si SCs (1.65%). Xie *et al.* prepared the Si hole array (SiHA) using

photolithography and reaction ion etching (RIE).⁹⁵ The surface of SiHA displayed a smooth texture, validating the presence of minimal surface recombination velocity. As illustrated in Fig. 7, the light absorption of SiHA intensified as the depth of the holes increased, underscoring its heightened light-trapping capabilities.^{94,95} Through the mixture of light trapping in SiHA and the utilization of AuCl₃ for graphene doping, researchers achieved a high PCE of 10.40%.^{94,95} These devices indicated remarkable stability, maintaining their increased efficiency even after being stored in ambient air for about 3 months.

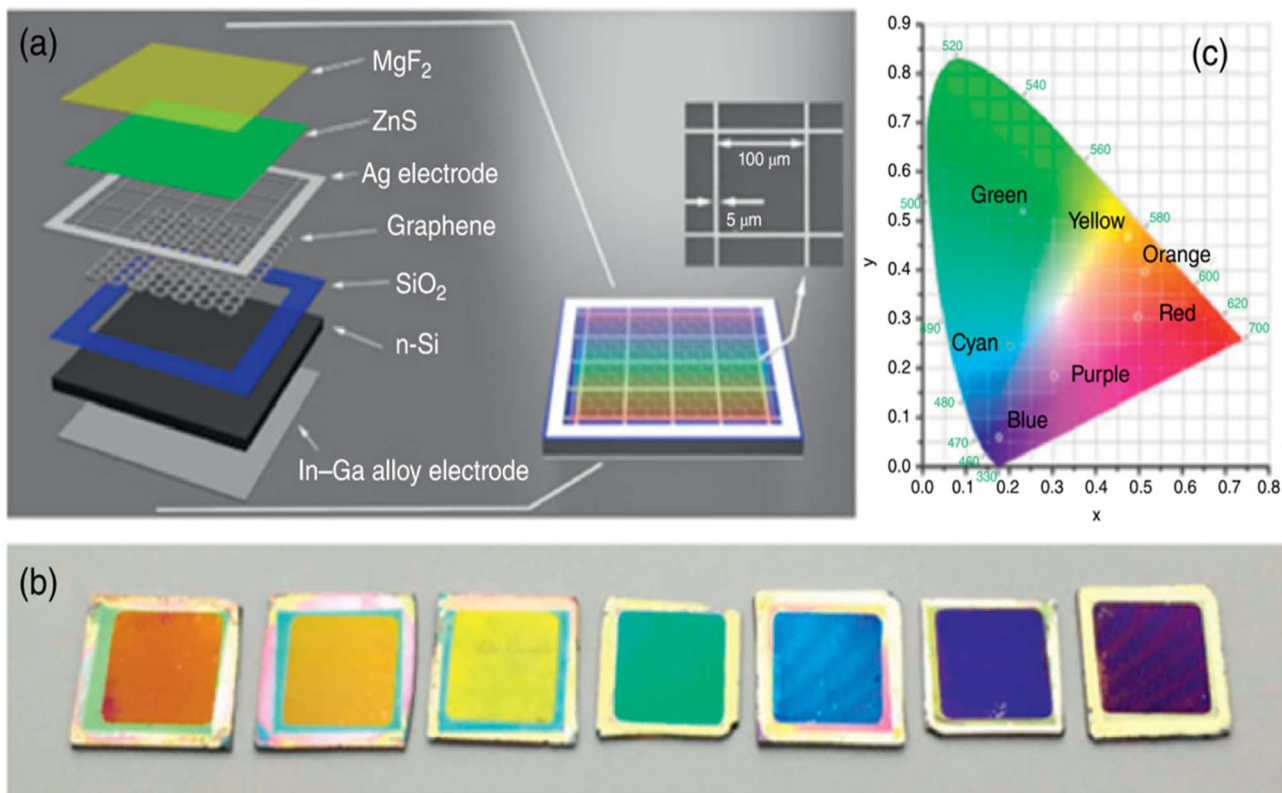


Fig. 9 G/Si SB-SCs with (a) schematic presentation of the color device, (b) photographs of device area: 1 cm^2 with various colors, and (c) coordinates of seven colors in CIE chromaticity. (a) and (b) Has been reproduced from ref. 99 with permission Elsevier.

6.3. Antireflection coating

Antireflection coating (ARC) is a method that uses a dielectric layer such as SiO_2 , TiO_2 to enhance the performance of G/Si solar cells by reducing the reflection of incident light at the surface of the Si. This layer is designed to optimize and minimize the loss of incoming photons owing to reflection, thereby increasing the amount of light that can be absorbed by the solar cells (Fig. 8a).⁹⁶ In the case of G/Si structures with an ARC, the resulting stack consists of four layers: air/ARC/G/Si. Fig. 8b indicates the refractive index of some of ARC candidate materials.⁹⁷ TiO_2 is a promising candidate for ARC due to its refractive index. However, the integration of TiO_2 film and graphene surface depends on the fabrication methods.⁹⁶ The physical deposition method with high energy can destroy the graphene while solution methods still maintain the pristine graphene. Instead, Shi *et al.*⁹⁷ prepared TiO_2 film by sol-gel method on G/Si SCs, as presented in Fig. 8a.⁹⁶ The results show that the reflectance was reduced to 10% (with TiO_2 film) compared to without TiO_2 , as indicated in Fig. 8c.⁹⁷ Fig. 8d compared the J - V characteristics of SCs with un-doped, HNO_3 -doped, and TiO_2 coated on HNO_3 -doped.⁹⁷ The J - V characteristics show that the PCE of SCs improve when SCs were doped and combined doping and coating ARC layer refractive polymers, like PMMA ($n = 1.5$), can be used as RAC for G/Si SCs because they are highly transparent to visible light. Despite having a low refractive index compared to inorganic ARC

materials, it has benefits including being very transparent to visible light, light in weight, bendable, and flexible. Additionally, PMMA is commonly employed as a foundation layer during the transfer of graphene. By repurposing PMMA as an ARC, the need for removing PMMA subsequent to the graphene transfer is obviated, simplifying the device production process. The performance of G/Si SCs was significantly improved by utilizing PMMA-coated graphene films contrasted to bare G/Si SCs that underwent PMMA elimination. Fig. 8e contrasts the reflectance spectra of PMMA eliminated G/Si and PMMA-G/Si devices, indicating that the PMMA-G/Si devices exhibit higher absorption capabilities.⁹⁸

Fig. 8f demonstrates the J_{SC} , FF, and PCE of PMMA extracted-G/Si and PMMA-G/Si SCs of 22.61 mA cm^{-2} , 32.22%, 3.12%, and 33.64 mA cm^{-2} , 45.56%, 6.55%, respectively.⁹⁹ In particular, the PCE of HNO_3 -doped PMMA-G/Si SCs up to 13.34%. It is noteworthy that the structure of PMMA was not affected by the HNO_3 doping, making the doping procedure of PMMA coated graphene convenient. Ding *et al.*¹⁰⁰ utilized double layered MgF_2/ZnS coating on G/Si SCs, serving a dual intention. Firstly, for Si SCs operating in the range of 380 to 1100 nm, ZnS and MgF_2 have higher ($n = 2.5$) and lower ($n = 1.4$) refractive indices, respectively. Therefore, the MgF_2/ZnS double layer served as an effective ARC. Secondly, by adjusting the thickness of ZnS and MgF_2 , different colors could be transmitted to G/Si SCs. The color tuning process for G/Si SCs was easy due to the transparent nature of graphene. Fig. 9 depicts the display, visuals,



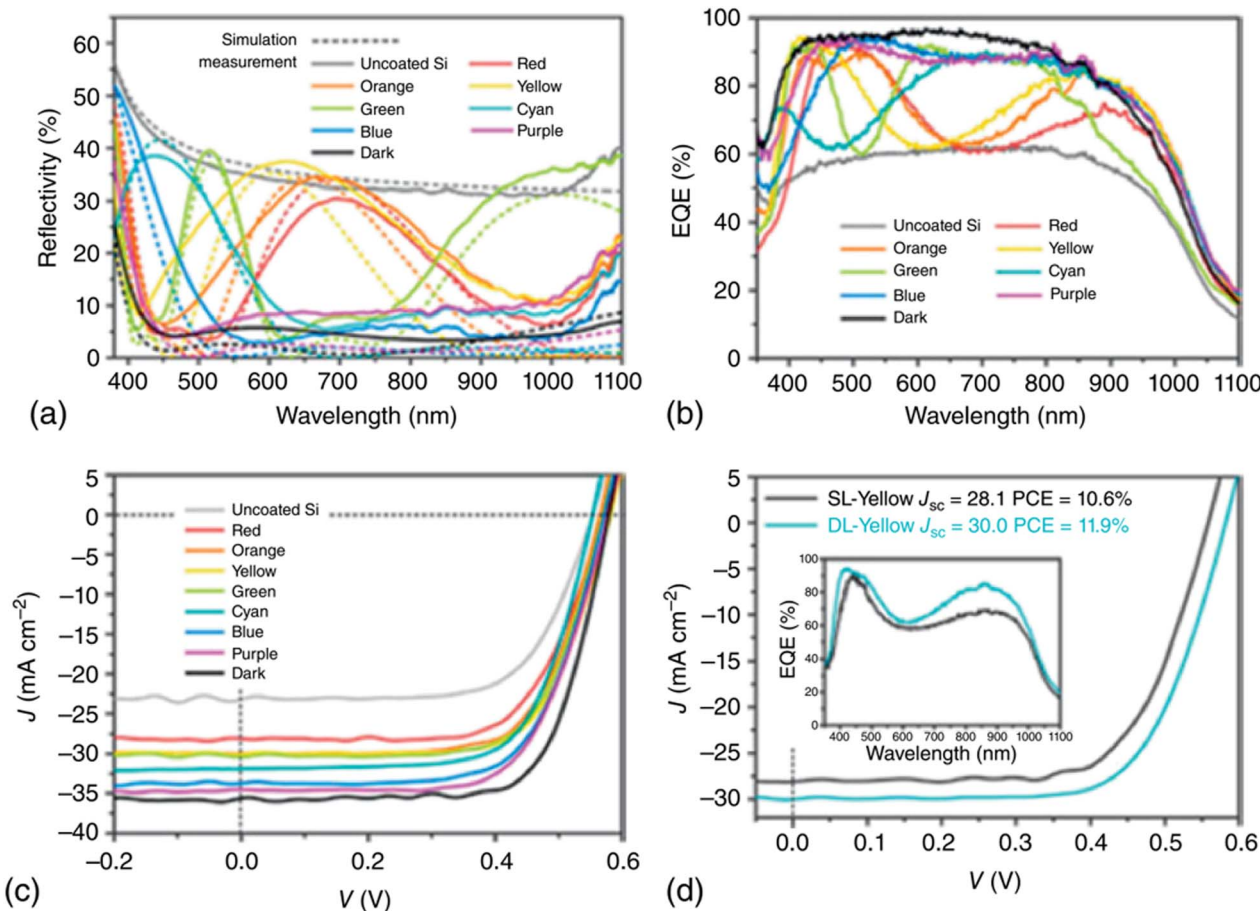


Fig. 10 (a) Modeled (dash lines) and observed (solid lines) reflection spectra of DL-MgF₂/ZnS-coated G/Si heterojunction SCs (b) EQE spectra of the uncoated and G/Si SCs with various structural colors, (c) J–V spectra of the devices with various structural colors. J–V spectra of the devices without coating and with enhanced anti-reflection coating were also indicated for comparison, (d) contrast of the J–V and EQE (inset) among SL-ZnS-coated and DL-MgF₂/ZnS-coated G/Si devices. (a)–(d) Have been reproduced from ref. 99 with permission from Elsevier.

and CIE chromaticity coordinates of seven colors for G/Si SCs with DL-MgF₂/ZnS films.¹⁰⁰

Fig. 10 illustrates the reflectance spectra of different colored MgF₂/ZnS coated G/Si SCs.⁹⁹ It is evident that the absorption was enhanced correlated to pristine G/Si SCs. Comparable trends were seen for the EQE spectra. Remarkably, the multi-color G/Si SCs achieved a high PCE of 10.7–13.2%.⁹⁹ By utilizing an enhanced MgF₂/ZnS antireflection layer, the PCE of the device reached an impressive value of 14.6%.⁹⁹

6.4. Influence of engineering

Despite numerous methods being used to enhance G/Si devices, their performance is still inferior to that of Si p–n SB-SCs used in commercial applications. This discrepancy primarily arises from the diminished built-in electric field in the SJ, which cannot effectively suppress carrier combinations along the interface. By overwhelming obstacle carriers (electron in n-Si) *via* inserting an interfacial barrier layer between graphene and Si, recombining electron/hole pairs can prevent and ought to support the transfer of holes to graphene. However, the types of materials and the thicknesses of the layers are a signify to the extensive study. Some thin film materials such as SiO₂, h-BN,

MoS₂, MoO₃, and P3HT have been utilized.^{101–105} If the layer is very thick, the ohmic inefficiencies can appear. On the other hand, the layer is too thin and may fail to block majority carriers' transport. Therefore, optimizing the dimension of the barrier layer is necessary to strike a balance between reducing carrier recombination and minimizing ohmic losses. Studies have shown that oxide layers with a thickness of lower than 2 nm can effectively passivate the interface, leading to increased V_{OC} and FF. By selecting the optimal oxide thickness (1.5 nm), a PCE of 12.4% was achieved through chemical doping. This efficiency further increased to 15.6% following the implementation of a TiO₂ ARC.^{101,102} The thickness of ultra-thin SiO₂, however, is difficult to adjust because it depends on the crystal orientation and external factors.

Recently, the insulating material of h-BN, an appealing choice as a barrier layer for G/Si SCs due to high transparency, dangling bond-free surface, and proper band alignment with n-Si substrate.¹⁰¹ Fig. 11 presents the band diagram of G/h-BN/Si SCs, highlighting the effects of h-BN insertion.¹⁰¹ It's clear that compared to a basic G/Si interface, the introduction h-BN creates a substantial barrier that impedes electron transfer at the interface.¹⁰² However, it simultaneously enables easy

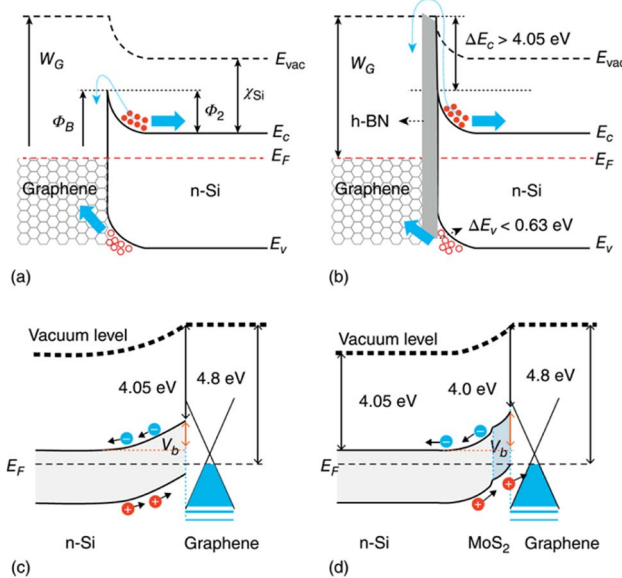


Fig. 11 Energy band diagrams of the G/Si SB-SCs (a) without and (b) with an h-BN electron blocking layer. (a) and (b) have been reproduced from ref. 102 with permission from Elsevier Presentations of band diagrams for the SCs. The PV procedures (c) in the graphene/n-Si and (d) in the graphene/MoS₂/n-Si SCs are indicated. (c) and d have been reproduced from ref. 101 with permission from Royal Society of Chemistry.

transport of holes from Si to graphene. Through the incorporation of the BN layer, PCE of the G/Si SCs attained 10.93%, which indicated a 15% efficient enhancement contrasted to the reference device.

Semiconductor layers with thickness (~ 50 nm) can be employed as barrier layers, offering a more convenient processing approach compared to insulators which require decreased thickness. MoS₂ thin film grown by different methods has been utilized as an interfacial barrier layer to improve PCE of SCs. The insertion of MoS₂ layer introduces a shift in the E_F , causing the lowest part of the CB and the top of VB of the MoS₂ layer at the interface of graphene to move upward, as shown in Fig. 11a-d.¹⁰¹ This creates an energy barrier at the interface between MoS₂ and n-Si and enhances the

entire energy barrier among graphene and n-Si. The additional energy barrier provided by the MoS₂ layer effectively blocks the photogenerated electrons in the Si, serving as an efficient electron-blocking layer. Alike band bending at the interface of the semiconductor barrier layer/n-Si interface has been noted in the cause of WO₃/n-Si structures.¹⁰¹ The substantial disparity in energy levels between the E_F of WO₃ and Si prompts a marked transfer of charges from Si, leading to a pronounced upward bending of the band at the interface of WO₃ and Si. Consequently, the built-in field (V_{bi}) of the G/Si SCs is improved inserting the WO₃ interlayer, leading to a notable improvement in PCE from 3.99% in G/Si SCs to 10.59%. Utilizing MoO₃ layers also contributed to elevating the PCE to 12.2% as a result of the significant ϕ_{wf} discrepancy in MoO₃, leading to the spontaneous injection of holes from the MoO₃ layer to Si.¹⁰¹ As a result of this hole injection process, a hole inversion layer is created at the surface of Si, generating a robust built-in electric field. This process effectively curbs recombination. Through additional device optimization steps involving graphene doping and the application of polymer anti-reflection coating, a high PCE of 12.2% was accomplished.

Organic semiconductors, P3HT also act as a hole transport layer and block the electron to reduce the recombination. Fig. 12 illustrates the band of P3HT and Si that LUMO and HUMO of P3HT are 3.2 and 5.1 eV, while the lowest conduction band and highest valence band are 4.05 and 5.17 eV.¹⁰⁶ This substantial offset allows the transport of holes, but it hinders the electrons. Optimized graphene/P3HT/Si NW array and graphene/P3HT/Si NH array devices achieved power conversion efficiencies of 9.94% and 10.34%, respectively.

A significant interaction at the interface between Si and MoO₃ layers has been noted, resulting in the remarkable attainment of PCE value of 12.2%. A substantial work ϕ_{wf} disparity was observed in MoO₃, leading to the spontaneous injection of holes from the MoO₃ layer to Si. This hole injection mechanism instigates the formation of a hole inversion layer on the Si surface and triggers the establishment of potent built-in electric field, effectively suppressing the recombination. Through additional device optimization steps involving graphene doping and the application of polymer anti-reflection coating, a high-PCE of 12.2% was accomplished.

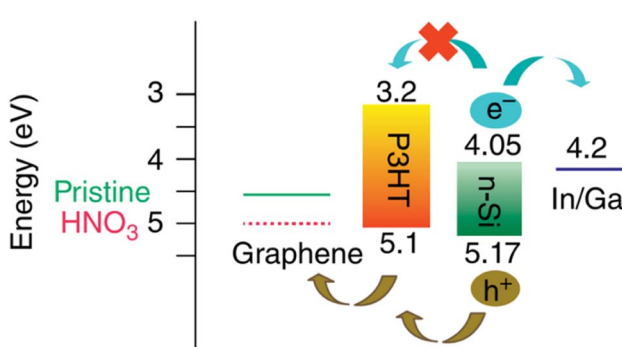


Fig. 12 Band diagram schematic of hybrid SCs. Figure has been reproduced from ref. 106 with permission from American Chemical Society.

6.5. Surface passivation

Surface passivation is another strategy to raise the PCE of SCs.¹⁰⁷⁻¹⁰⁹ As a result of the numerous dangling bonds on the Si surface, numerous surface states serve as recombination hubs. Recombination has a significant impact on the performance of G/Si and PV devices. The diffusion channel of the carrier can be improved to prevent recombination by dangling bond reduction on the Si surfaces. Various chemical entities, including hydrogen (H^-), methyl (CH_3^-), and oxide (SiO_x), have the potential to serve as passivation agents for Si surface.^{110,111} Hydrogen-passivated Si surfaces have garnered significant attention in the research literature due to their remarkable ability to passivate effectively (causing a substantial reduction in surface states by multiple orders of magnitude) and exhibit



an exceptionally low surface recombination velocity.^{110,112,113} Among them, oxide SiO_x shows the most chemical stability while H^- termination exhibits low chemical stability and is incompatible with graphene leading to Schottky barrier decrease.¹¹⁴ However, the compatibility of CH_3^- group leads to the increase in the Schottky that they are better for SC efficiency improvement. The result shows that passivation on Si surface exhibits the PCE of 1.41%, 1.76%, and 4.42% with H^- , CH_3^- , and oxide passivation, respectively.¹¹⁴ Other passivation layers such as modified SiO_2 , Al_2O_3 , HfO_2 , GO, P3HT, and SiN_x are also used to improve the SC efficiency.^{87,115-117}

6.6. Influence of encapsulation

Although the integrated G/Si heterojunctions in solar cells have achieved a lot of good results. However, another problem in the design and produce G/Si solar cells is also extremely important, that related to encapsulation of device to avoid and protect individual solar cells modules from various environmental factors and mechanical stress by enclosing them within protective materials and structures. In a report of Matacena *et al.* has used HNO_3 as a doping source to improve the performance of G/Si heterojunction solar cells.¹¹⁸ Simultaneously, the author has also been compared with/without encapsulated by ethylene-vinyl acetate (EVA). The results from C-V analysis are confirm that encapsulation avoids the fading of HNO_3 beneficial effects while it did not worse cells performance. In another innovation, Kim *et al.* has applied a protective layer for silver nanowires (Ag NWs) by graphene.¹¹⁹ In this work, the author designed the encapsulated graphene/Ag NWs/graphene for Schottky-type Si heterojunction solar cells. With this structure, the author has obtained a highest PCE of 3.51%, and it lost only 6.4% of its original PCE value after 30 days by employing the encapsulation layer, much less compared to the solar cells without the encapsulation. Since, G/Si solar cells encapsulation is vital part of PV module manufacturing, aimed at protecting the solar cells and ensuring the long-term performance and reliability of solar panels. Proper encapsulation helps extend the lifespan of solar modules and allows them to operate efficiently in a wide range of environment.

7. Conclusion, challenges, and perspectives

In general, owing to its exclusive characteristics, graphene has been recognized as an outstanding material for various solar energy harvesting devices. Its unique characteristics hold the promise of being efficient, environment-friendly, and inexpensive after a decade of devoted research and in-depth scientific discoveries. But there are still many perspectives and challenges ahead.

With its numerous advantages as a component of an SC, it possesses some limitations that can hinder it from being considered one of the best materials for an efficient SC. Graphene is widely regarded as a pivotal conductor of electricity, but it lacks a band gap in its molecular orbital structure, a shortcoming that researchers have been working to rectify

over the years. Once this limitation is overcome, graphene can serve as an exceptionally efficient anode in virtually any type of SCs. Another challenge associated with graphene is its susceptibility to oxidation in oxidative environments. This oxidation leads to structural changes that subsequently impact its chemical properties. Efforts are underway to develop strategies to mitigate the effects of oxidation and enhance graphene's stability. Despite these challenges, researchers are actively working to overcome these limitations and harness the full potential of graphene for SC applications. The chemical alterations and structural changes that can occur in graphene pose a significant challenge when considering large-scale energy production. Moreover, graphene exhibits some toxic properties, which is a matter that requires to be carefully examined in its development. Secondary cells typically have two electrodes, whereas SCs have only one electrode. This creates two main issues: changes in the ϕ_{wf} value and the direction of electron flow. The electron flow system in a SC with only one electrode is complex, and maintaining the integrity of the entire process is a significant task. Researchers have attempted to modify the ϕ_{wf} to address this challenge but altering the ϕ_{wf} of a specific material is a difficult endeavor. Aside from this persisting issue, it has been discovered that depositing graphene electrodes into the solar setup has proven to be a difficult task. The bottom of a graphene electrode is deposited on a substrate material (usually glass or elastomers) that acts as the foundation makes up for the SCs.¹²⁰ Owing to the poor dispersion properties of graphene, water is used as an appropriate solvent during this deposition process. However, various organic solvents are being tested to replace water in order to achieve a higher degree of dispersion. In typical graphene-induced SCs, when integrated into an n-Si SB-SCs with AM 1.5 illumination, it demonstrates a PCE of 8.6%. This value can be increased 4.5 times when doping the SC material. To achieve this, graphene is doped with ionic liquids such as bistriflimide, bis(trifluoromethanesulfonyl)amide, and others.¹²¹⁻¹²³ The doping process alters the chemical potential of graphene, leading to an increased carrier density, ultimately elevating the built-in potential of the SCs. This, in turn, enables a longer cell lifespan compared to traditional SCs. Recent approaches in optimizing G/Si SB-SCs were developed. These strategies can be divided into optimizing (i) the ϕ_{wf} and conductivity of graphene, (ii) Si's reflectivity, and (iii) modifying the G/Si interface. Through the implementation of these strategies, the PCE has risen from 1.5% to 15.8% in less than 10 years. Despite the fast advancements in this area, there are remaining matters that require further attention.

Firstly, various strategies have been explored to improve the PCE of SCs including passivation and band-engineering of the G/Si interface, insertion of an antireflection layer or nano-micro structures in enhancing the light harvest, the control of the number of graphene layers, and the chemical doping of graphene which has been confirmed to be the most efficient method for optimizing SC performance. Despite the introduction of numerous doping dopants, the durability of SCs remains a challenging issue due to the unsteadiness of the doping process. An increased stable single-walled carbon nanotube



(SWa-CNT)/Si SCs with a PCE greater than 11% after 10 months of ambient encounter was demonstrated.¹²⁴ By inserting a GO interlayer to develop a G/Si interface, new structure of G/GO/Si SC occupies 95% of its original level after one week of storage in the open air.¹²⁵ Similarly, an Al₂O₃ interlayer was inserted by Rehman *et al.*¹¹⁵ among the graphene and Si to inhibit the surface charge recombination at the interface, and their SC maintained its efficiency without degradation even after 9 months of exposure to ambient air. Initially, chemical doping of graphene led to a significant deterioration of G/Si SCs. Recently, GO demonstrated some PCE durability where Yavuz *et al.* published the degradation in PCE less than 1% after 3 weeks.^{79,126} Nevertheless, more research into the stability under various parameters, such as humidity and temperature, is needed. Moreover, alternative materials such as a CNT-oxide-Si cell with a PDMS anti-reflective coating were employed to reveal a small drop in efficiency from 10.9% to 9.1% in air over 20 days. Thus, materials with high durability, like CNTs, can be utilized to

ensure the stability of a SC. Investigating new SC structures, such as introducing an interlayer to engineer G/Si interface to create a metal–insulator–semiconductor (MIS) structure, could also be a vital direction in this field.

Secondly, although the PCE of G/Si SCs managed 15.8% in a few years, it still falls short of the PCE achieved by commercially available Si-p-n junction SCs. One of the limitations contributing to this is the decreased electrical conductivity and ϕ_{wf} of graphene. As a result, the energetic region of current studies involving G/Si SCs is relatively small ($<10 \text{ mm}^2$). Researchers demonstrated the device performance in various device areas from 4 to 100 mm². Interestingly, the PCE decreased from 10.56% to 3.62%, with an increase in the device area. This reduction in efficiency can be attributed to series resistance, which influences performance of SCs at larger scales. This result underscores the direct relationship between the energetic region of a SC and its overall behavior.¹²⁷ Furthermore, it has been reported in another study that the PCE

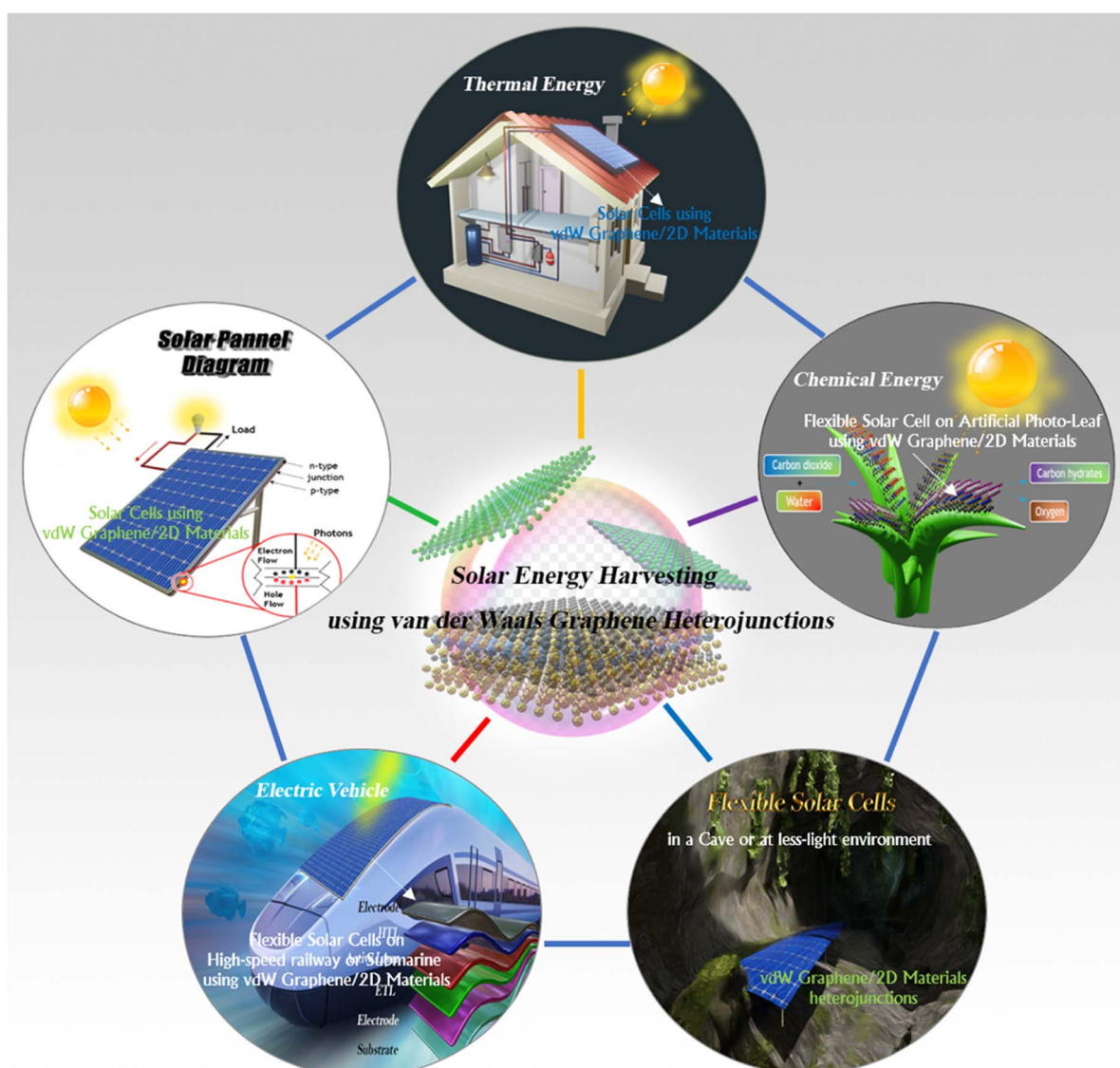


Fig. 13 The promising prospects of van der Waals graphene heterojunctions integrated into the solar energy harvesting.



of G/Si SCs lowered from 14.5% to 10.6% as the active region raised from 4.7 mm^2 to 14.5 mm^2 .⁹⁷ However, through interface engineering, it has been demonstrated that G/Si SCs can reach a PCE over 7% with a device region of 0.09 cm^2 .¹²⁵ It is essential to raise the active area to a minimum of 0.1 cm^2 for further improvement. Due to high sheet resistance of the graphene layer, the collection efficiency of photogenerated charge carriers would be decreased with a larger size of the device's active area. A grid electrode has been introduced to the traditional window-based device structure to reduce the resistance of graphene layer.¹²⁸ This grid electrode design facilitates low-resistance contact with the graphene layer and enhances carrier collection efficiency. Therefore, employing a fine metal electrode design on the front side is essential to favor carrier collection throughout the entire device region. Another significant matter is the long-term durability of these G/Si SCs. With the passage of time, the performance of these SCs begins to deteriorate, particularly after the doping process. A number of researchers have studied the durability of G/Si SCs during storage and attempted to mitigate the deterioration. Xie *et al.*⁹⁵ noted outcomes after various time intervals, indicating that the PCE of G/Si SCs decreased from 10.40% to 7.42% within 3 months.

Third, graphene is commonly moved on a Si substrate to create an SJ. However, graphene is fragile, and the remaining copper particles may stay on the graphene film after wet etching.^{129,130} These contaminants at the G/Si interface can act as short-circuit channels, resulting in current loss. As expected, the leakage current becomes more prominent as the device area increases. Therefore, the increased area of graphene is an important parameter affecting collection efficiency. To address this issue, advanced manufacturing and transfer skills must be addressed to reduce the flaws and contaminants encountered during the wet transfer method. Additionally, an alternative approach involves directly growing graphene on the semiconductor surface, resulting in a more uniform graphene with fewer structural defects.¹³¹

On the other hand, G/Si PVs are progressing in large-scale integration, offering high-efficiency and sustained solar technologies.⁸⁴ Nevertheless, the performance of G/n-Si single-junction cells falls short compared with that of p-n junction of SCs due to some main causes, such as low Schottky barrier height, transfer-based SC design, and high lateral resistivity of graphene. The interfacial barrier height of G/n-Si SCs is $\phi_G - \phi_{SBH} = \phi_G - \chi_{n-Si} = 0.65\text{ eV}$ which is lower than the Si energy bandgap (1.1 eV at 300 K). The G/Si SC designs evolved by moving graphene onto the Si substrates through a polymer-film-based chemical-transfer procedure. This process can cause defect centers, exacerbating interfacial carrier recombination and ultimately lowering the PV performance. The mobility of charge carriers of layer graphene grown by CVD is better than other methods. Nevertheless, a single graphene layer has a higher sheet resistance ($100\text{--}100\text{ }\Omega^{-1}$) than the solar-grade doped Si ($50\text{--}100\text{ }\Omega^{-1}$) of the p-n junction SCs.¹³² Such high lateral resistivity of graphene films results in inefficient losses such as increased R_s and decreased fill factors in G/Si PV heterojunction cells. Several approaches to overcoming the challenges of G/Si PV devices have been explained.⁸⁴ The following

part outlines strategies for tuning the interface utilizing suitable interlayers and modulating the functionality of graphene, all aimed at reaching highly efficient and robust G/Si SCs.

Graphene's impact on the field of solar energy harvesting devices is not limited to revolutionizing renewable energy assets. It is also a promising material for smart energy generation and storage devices. Nevertheless, conventional energy generators are incapable of providing responses to environmental changes and traditional energy storage devices lack functionalities other than providing electricity, posing challenges. However, graphene owing to its microscopic structure modification and exceptional physicochemical properties offers potential solutions to these issues. Thus, intelligent energy generation and storage and smart electric devices that can engage with receptive to external stimuli are becoming increasingly important and highly demanded. Recently, the key advances that involve the integration of graphene into smart energy generation and storage systems were systematically reviewed by Ye *et al.*¹³³ In the context of smart energy generation, the authors discussed graphene-derived electric generators that can harvest electricity in response to external stimuli, such as flowing liquid, moisture, pressure force, friction, and heat. These advanced energy storage solutions exhibit remarkable features such as wearability, deformability, printability, responsiveness to stimuli, integration capabilities, miniaturization, and self-healing properties, showcasing the exciting possibilities enabled by graphene in the realm of energy storage.

Industrial production has been extremely high with a massive global demand for graphene-based commercial products. In PVs, graphene has been discovered as an electrode in SC technologies thanks to its brilliant properties. Recent advancements in G/Si-based (SB-SCs) have received considerable attention. With the noble continued efforts of researchers, the PCE for G/Si SCs has dramatically increased from 1.65% to 15%, which is comparable to that of metal halide perovskite cells with the highest efficiency of 20–22%.¹³⁴ However, there is a great opportunity for enhancement in the behavior of G/Si SCs. To improve the overall PCE of G/Si SCs, chemical doping of graphene, interfacial layer utilization, and anti-reflection coatings have played significant roles. The surface recombination in influencing FF was expanded with prominence on the passivation approach and the use of a thin hole transport interlayer. All parameters such as J_{SC} , V_{OC} , and FF, eventually establish the PCE of certain G/Si SCs. In perceptions, G/Si appears to offer new utilizations for future-generation SCs. Despite its fast progress, there are challenges and limitations to its implementation on a commercial scale. One of the major challenges lies in achieving continuous graphene growth with excellent material quality. Additionally, the environmental durability of G/Si SCs is a concern. However, recent advancements suggest that graphene-based electronics combined with Si can lead to high-efficiency SCs with commercial viability. Therefore, G/Si heterostructure systems demonstrate industrial potential, as efforts are being made to reduce costs and capitalize on their lightweight nature and corrosion resistance, making them an ideal material for PVs. Several companies and



research institutes are now emphasizing on graphene chemistry R&D to enhance the efficiency and production of induced graphene in SCs. Following the successful implementation of graphene electrodes in the SC, various other electronic entities are exploring improving graphene in their machinery in order to reach the same level of efficiency in those sectors. The automotive industry can become more environmentally friendly by incorporating SCs, which enhance the speed and range of solar cars. In conclusion, graphene-induced SCs are considered one of the most significant inventions of this decade, capturing the attention and driving the development of the global scientific community. Furthermore, scientists are actively working towards enhancing the efficiency of graphene-based SCs to maximize energy harnessing. By promoting solar energy, graphene holds a key role in facilitating sustainable, clean, and environmentally friendly energy productions and utilization worldwide (Fig. 13). Importantly, graphene's success extends beyond SCs to encompass various notable applications, including sensors, photodetectors, and smart energy generation and storage devices.

Author contributions

Top Khac Le: investigation, writing – original draft. The-Hung Mai: writing – original draft. Muhammad Aamir Iqbal: writing – original draft. Dimitra Vernardou: writing – original draft. Van Duong Dao: writing – original draft. Vinoth Kumar Ponnusamy: investigation, writing – original draft. Chandra Sekhar Rout: investigation, writing – original draft. Phuong V. Pham: resources, project administration, funding acquisition, conceptualization, methodology, investigation, writing – original draft, writing – review & editing.

Conflicts of interest

The authors declare that they have no known competing financial interests or personal relationships that could have appeared to influence the work reported in this paper.

Acknowledgements

The authors acknowledge the supports from the National Science and Technology Council, Taiwan (Grant No. NSTC-112-2112-M-110-004-MY3), the Research Center for Precision Environmental Medicine, Kaohsiung Medical University, Kaohsiung, Taiwan from The Featured Areas Research Center Program within the framework of the Higher Education Sprout Project by the Ministry of Education (MOE) in Taiwan and by Kaohsiung Medical University Research Center Grant (KMUTC112A01), and the grant MOST-110-2113-M-037-009- from the Ministry of Science and Technology, Taiwan.

References

- 1 B. Parida, S. Yoon, S. M. Jeong, J. S. Cho, J. K. Kim and D. W. Kang, *Sol. Energy Mater. Sol. Cells*, 2020, **204**, 110212.
- 2 K. Yoshikawa, H. Kawasaki, W. Yoshida, T. Irie, K. Konishi, K. Nakano, T. Uto, D. Adachi, M. Kanematsu, H. Uzu and K. Yamamoto, *Nat. Energy*, 2017, **2**, 17032.
- 3 M. Nakamura, K. Yamaguchi, Y. Kimoto, Y. Yasaki, T. Kato and H. Sugimoto, *IEEE J. Photovoltaics*, 2019, **9**, 1863–1867.
- 4 N. Yan, C. Zhao, S. You, Y. Zhang and W. Li, *Chin. Chem. Lett.*, 2020, **31**, 643–653.
- 5 W. Shi and X. Ma, *Coatings*, 2018, **8**, 2.
- 6 V. P. Pham and G. Y. Yeom, *Adv. Mater.*, 2016, **28**, 9024–9059.
- 7 P. V. Pham, S. Chanakya Bodepudi, K. Shehzad, Y. Liu, Y. Xu, B. Yu and X. Duan, *Chem. Rev.*, 2022, **122**, 6514–6613.
- 8 C. H. Lee, G. H. Lee, A. M. Van DerZande, W. Chen, Y. Li, M. Han, X. Cui, G. Arefe, C. Nuckolls, T. F. Heinz, J. Guo, J. Hone and P. Kim, *Nat. Nanotechnol.*, 2014, **9**, 676–681.
- 9 M. Shanmugam, R. Jacobs-Gedrim, E. S. Song and B. Yu, *Nanoscale*, 2014, **6**, 12682–12689.
- 10 T. Saga, *NPG Asia Mater.*, 2010, **2**, 96–102.
- 11 K. S. Novoselov, A. K. Geim, S. V. Morozov, D. Jiang, Y. Zhang, S. V. Dubonos, I. V. Grigorieva and A. A. Firsov, *Science*, 2004, **306**, 666–669.
- 12 A. K. Geim and K. S. Novoselov, *Nat. Mater.*, 2007, **6**, 183–191.
- 13 A. A. Balandin, *Nat. Mater.*, 2011, **10**, 569–581.
- 14 T. Mahmoudi, Y. Wang and Y. B. Hahn, *Nano Energy*, 2018, **47**, 51–65.
- 15 Q. Zheng, Z. Li, J. Yang and J. K. Kim, *Prog. Mater. Sci.*, 2014, **64**, 200–247.
- 16 A. DiBartolomeo, *Phys. Rep.*, 2016, **606**, 1–58.
- 17 G. Luongo, A. Grillo, F. Giubileo, L. Iemmo, M. Lukosius, C. A. Chavarin, C. Wenger and A. DiBartolomeo, *Nanomaterials*, 2019, **9**, 659.
- 18 B. Partoens and F. M. Peeters, *Phys. Rev. B: Condens. Matter Mater. Phys.*, 2006, **74**, 075404.
- 19 P. V. Pham, *The New Etching Technologies of Graphene Surfaces*, IntechOpen, 2020, DOI: [10.5772/intechopen.92627](https://doi.org/10.5772/intechopen.92627).
- 20 P. Pham, P. Goel, S. Kumar and K. Yadav, *21st Century Surface Science - A Handbook*, IntechOpen, 2020, DOI: [10.5772/intechopen.87891](https://doi.org/10.5772/intechopen.87891).
- 21 P. V. Pham, *21st Century Nanostructured Materials - Physics, Chemistry, Classification, and Emerging Applications in Industry, Biomedicine, and Agriculture*, IntechOpen, 2022, DOI: [10.5772/intechopen.94802](https://doi.org/10.5772/intechopen.94802).
- 22 K. A. A. Min-Dianey, T. K. Le, J. R. Choi and P. V. Pham, *Nanomaterials*, 2021, **11**, 816.
- 23 K. A. A. Min-Dianey, T. K. Le, A. Qadir, N. L. P. M'bouana, M. Malik, S. W. Kim, J. R. Choi and P. V. Pham, *Nanomaterials*, 2021, **11**, 2934.
- 24 U. Farooq, K. A. A. Min-Dianey, P. Rajagopalan, M. Malik, D. Mani Kongnine, J. R. Choi and P. V. Pham, *Nanomaterials*, 2022, **12**, 712.
- 25 M. A. Iqbal, M. Malik, W. Shahid, W. Ahmad, K. A. A. Min-Dianey, P. V. Pham, *Plasmonic 2D Materials: Overview, Advancements, Future Prospects and Functional Applications*, IntechOpen, 2021, DOI: [10.5772/intechopen.101580](https://doi.org/10.5772/intechopen.101580).



26 P. V. Pham, *Atmospheric Pressure Chemical Vapor Deposition of Graphene*, IntechOpen, 2018, DOI: [10.5772/intechopen.81293](https://doi.org/10.5772/intechopen.81293).

27 V. P. Pham, *Direct Growth of Graphene on Flexible Substrates Toward Flexible Electronics: A Promising Perspective*, IntechOpen, London, UK, 2017.

28 V. P. Pham, H. S. Jang, D. Whang and J. Y. Choi, *Chem. Soc. Rev.*, 2017, **46**, 6276–6300.

29 P. V. Pham, *R. Soc. Open Sci.*, 2018, **5**, 1–6.

30 A. Qadir, T. K. Le, M. Malik, K. Aniya, A. Min-Dianey, I. Saeed, Y. Yu, J. R. Choi and P. V. Pham, *RSC Adv.*, 2021, **11**, 23860–23880.

31 M. Malik, M. A. Iqbal, J. R. Choi and P. V. Pham, *Front. Chem.*, 2022, **10**, 905404.

32 P. V. Pham, *ACS Omega*, 2018, **3**, 8036–8041.

33 G. A. Nowsherwan, A. Samad, M. A. Iqbal, T. Mushtaq, A. Hussain, M. Malik, S. Haider, P. V. Pham and J. R. Choi, *Nanomaterials*, 2022, **12**, 1767.

34 M. A. Iqbal, N. Anwar, M. Malik, M. Al-Bahrani, M. R. Islam, J. R. Choi, P. V. Pham and X. Liu, *Adv. Mater. Interfaces*, 2023, **10**, 2202208.

35 M. Aamir Iqbal, M. Malik, T. Khac Le, N. Anwar, S. Bakhsh, W. Shahid, S. Shahid, S. Irfan, M. Al-Bahrani, K. Morsy, H.-B. Do, V. Kumar Ponnusamy and P. V. Pham, *ACS Mater. Lett.*, 2023, **5**, 1027–1060.

36 V. P. Pham, K. H. Kim, M. H. Jeon, S. H. Lee, K. N. Kim and G. Y. Yeom, *Carbon*, 2015, **95**, 664–671.

37 V. P. Pham, A. Mishra and G. Young Yeom, *RSC Adv.*, 2017, **7**, 16104–16108.

38 K. N. Kim, V. P. Pham and G. Y. Yeom, *ECS J. Solid State Sci. Technol.*, 2015, **4**, N5095–N5097.

39 V. P. Pham, D. S. Kim, K. S. Kim, J. W. Park, K. C. Yang, S. H. Lee, G. Y. Yeom and K. N. Kim, *Sci. Adv. Mater.*, 2016, **8**, 884–890.

40 V. P. Pham, M. T. Nguyen, J. W. Park, S. S. Kwak, D. H. T. Nguyen, M. K. Mun, H. D. Phan, D. S. Kim, K. H. Kim, N. E. Lee and G. Y. Yeom, *2D Mater.*, 2017, **4**, 025049.

41 V. P. Pham, K. N. Kim, M. H. Jeon, K. S. Kim and G. Y. Yeom, *Nanoscale*, 2014, **6**, 15301–15308.

42 P. V. Pham, *C*, 2018, **4**, 34.

43 F. Bonaccorso, Z. Sun, T. Hasan and A. C. Ferrari, *Nat. Photonics*, 2010, **4**, 611–622.

44 L. A. Falkovsky, *J. Phys.: Conf. Ser.*, 2008, **129**, 012004.

45 R. R. Nair, P. Blake, A. N. Grigorenko, K. S. Novoselov, T. J. Booth, T. Stauber, N. M. R. Peres and A. K. Geim, *Science*, 2008, **320**, 1308.

46 A. Altunete, A. Seyhan and R. Zan, *J. Mol. Struct.*, 2020, **1200**, 127055.

47 S. Pang, Y. Hernandez, X. Feng and K. Müllen, *Adv. Mater.*, 2011, **23**, 2779–2795.

48 X. Li, H. Zhu, K. Wang, A. Cao, J. Wei, C. Li, Y. Jia, Z. Li, X. Li and D. Wu, *Adv. Mater.*, 2010, **22**, 2743–2748.

49 Y. J. Yu, Y. Zhao, S. Ryu, L. E. Brus, K. S. Kim and P. Kim, *Nano Lett.*, 2009, **9**, 3430–3434.

50 C. Ö. Girit, J. C. Meyer, R. Erni, M. D. Rossell, C. Kisielowski, L. Yang, C. H. Park, M. F. Crommie, M. L. Cohen, S. G. Louie and A. Zettl, *Science*, 2009, **323**, 1705–1708.

51 C. Lee, X. Wei, J. W. Kysar and J. Hone, *Science*, 2008, **321**, 385–388.

52 G. Fiori, F. Bonaccorso, G. Iannaccone, T. Palacios, D. Neumaier, A. Seabaugh, S. K. Banerjee and L. Colombo, *Nat. Nanotechnol.*, 2014, **9**, 768–779.

53 U. Mehmood, H. Asghar, F. Babar and M. Younas, *Sol. Energy*, 2020, **196**, 132–136.

54 G. Jeong, D. Koo, J. Seo, S. Jung, Y. Choi, J. Lee and H. Park, *Nano Lett.*, 2020, **20**, 3718–3727.

55 W. Liao, Y. Gao, W. Wang, X. Zuo, Q. Yang, Y. Lin, H. Tang, S. Jin and G. Li, *ACS Sustainable Chem. Eng.*, 2020, **8**, 7308–7315.

56 M. Kim, M. A. Rehman, K. M. Kang, Y. Wang, S. Park, H. S. Lee, S. B. Roy, S. H. Chun, C. A. Singh, S. C. Jun and H. H. Park, *Appl. Mater. Today*, 2022, **26**, 101267.

57 S. Aftab, M. Z. Iqbal, S. Alam and M. Alzaid, *Int. J. Energy Res.*, 2021, **45**, 18173–18181.

58 X. Li, W. Chen, S. Zhang, Z. Wu, P. Wang, Z. Xu, H. Chen, W. Yin, H. Zhong and S. Lin, *Nano Energy*, 2015, **16**, 310–319.

59 T. Mahmoudi, Y. Wang and Y. B. Hahn, *Adv. Energy Mater.*, 2020, **10**, 1903369.

60 E. Lamanna, F. Matteocci, E. Calabro, L. Serenelli, E. Salza, L. Martini, F. Menchini, M. Izzi, A. Agresti, S. Pescetelli, S. Bellani, A. E. DelRío Castillo, F. Bonaccorso, M. Tucci and A. DiCarlo, *Joule*, 2020, **4**, 865–881.

61 Z. Shi and H. Jayatissa, *Materials*, 2017, **11**, 36.

62 Y. Ye, L. Dai, P. C. Wu, C. Liu, T. Sun, R. M. Ma and G. G. Qin, *Nanotechnology*, 2009, **20**, 375202.

63 D. Wei and J. Kivioja, *Nanoscale*, 2013, **5**, 10108–10126.

64 D. Zhang, L. Gan, Y. Cao, Q. Wang, L. Qi and X. Guo, *Adv. Mater.*, 2012, **24**, 2715–2720.

65 F. Chen, Q. Qing, J. Xia, J. Li and N. Tao, *J. Am. Chem. Soc.*, 2009, **131**, 9908–9909.

66 P. Wadhwa, G. Seol, M. K. Petterson, J. Guo and A. G. Rinzler, *Nano Lett.*, 2011, **11**, 2419–2423.

67 A. L. Walter, K. J. Jeon, A. Bostwick, F. Speck, M. Ostler, T. Seyller, L. Moreschini, Y. S. Kim, Y. J. Chang, K. Horn and E. Rotenberg, *Appl. Phys. Lett.*, 2011, **98**, 2011–2014.

68 J. T. Robinson, J. S. Burgess, C. E. Junkermeier, S. C. Badescu, T. L. Reinecke, F. K. Perkins, M. K. Zalalutdinov, J. W. Baldwin, J. C. Culbertson, P. E. Sheehan and E. S. Snow, *Nano Lett.*, 2010, **10**, 3001–3005.

69 S. Chandramohan, V. Janardhanam, T. H. Seo, C. H. Hong and E. K. Suh, *Mater. Lett.*, 2019, **246**, 103–106.

70 L. Xiao, Y. Xu, A. A. Hakro, A. Hasan, R. Hao, B. Zhang and H. Chen, *J. Mater. Chem. C*, 2013, **1**, 1618–1627.

71 X. Li, Y. Zhu, W. Cai, M. Borysiak, B. Han, D. Chen, R. D. Piner, L. Colombo and R. S. Ruoff, *Nano Lett.*, 2009, **9**, 4359–4363.

72 T. Feng, D. Xie, Y. Lin, Y. Zang, T. Ren, R. Song, H. Zhao, H. Tian, X. Li, H. Zhu and L. Liu, *Appl. Phys. Lett.*, 2011, **99**, 233505.



73 Y. Song, X. Li, C. Mackin, X. Zhang, W. Fang, T. Palacios, H. Zhu and J. Kong, *Nano Lett.*, 2015, **15**, 2104–2110.

74 A. H. Castro Neto, F. Guinea, N. M. R. Peres, K. S. Novoselov and A. K. Geim, *Rev. Mod. Phys.*, 2009, **81**, 109–162.

75 T. Cui, R. Lv, Z. H. Huang, S. Chen, Z. Zhang, X. Gan, Y. Jia, X. Li, K. Wang, D. Wu and F. Kang, *J. Mater. Chem. A*, 2013, **1**, 5736–5740.

76 X. Miao, S. Tongay, M. K. Petterson, K. Berke, A. G. Rinzler, B. R. Appleton and A. F. Hebard, *Nano Lett.*, 2012, **12**, 2745–2750.

77 X. Li, L. Fan, Z. Li, K. Wang, M. Zhong, J. Wei, D. Wu and H. Zhu, *Adv. Energy Mater.*, 2012, **2**, 425–429.

78 X. Li, D. Xie, H. Park, M. Zhu, T. H. Zeng, K. Wang, J. Wei, D. Wu, J. Kong and H. Zhu, *Nanoscale*, 2013, **5**, 1945–1948.

79 S. Yavuz, C. Kuru, D. Choi, A. Kargar, S. Jin and P. R. Bandaru, *Nanoscale*, 2016, **8**, 6473–6478.

80 K. Huang, Y. Yan, X. Yu, H. Zhang and D. Yang, *Nano Energy*, 2017, **32**, 225–231.

81 M. F. Bhopal, D. Won Lee, S. H. Lee, A. R. Lee, H. J. Kim and S. H. Lee, *Mater. Lett.*, 2019, **234**, 237–240.

82 C. Kuru, S. Yavuz, A. Kargar, D. Choi, C. Choi, C. Rustomji, S. Jin and P. R. Bandaru, *J. Nanosci. Nanotechnol.*, 2016, **16**, 1190–1193.

83 K. Huang, X. Yu, J. Cong and D. Yang, *Adv. Mater. Interfaces*, 2018, **5**, 1801520.

84 M. F. Bhopal, D. W. Lee, A. U. Rehman and S. H. Lee, *J. Mater. Chem. C*, 2017, **5**, 10701–10714.

85 T. Feng, D. Xie, Y. Lin, H. Zhao, Y. Chen, H. Tian, T. Ren, X. Li, Z. Li, K. Wang, D. Wu and H. Zhu, *Nanoscale*, 2012, **4**, 2130–2133.

86 M. Abdullah-Al-Galib, B. Hou, T. Shahriadi, S. Zivanovic and A. D. Radadia, *Appl. Surf. Sci.*, 2016, **366**, 78–84.

87 J. Ahn, H. Chou and S. K. Banerjee, *J. Appl. Phys.*, 2017, **121**, 163105.

88 X. Li, Z. Lv and H. Zhu, *Adv. Mater.*, 2015, **27**, 6549–6574.

89 X. Liu, X. W. Zhang, Z. G. Yin, J. H. Meng, H. L. Gao, L. Q. Zhang, Y. J. Zhao and H. L. Wang, *Appl. Phys. Lett.*, 2014, **105**, 183901.

90 S. Chandramohan, S. Durairaj, T. H. Seo, B. D. Ryu and C. H. Hong, *J. Appl. Phys.*, 2021, **129**, 13101.

91 X. Wang, J. BinXu, W. Xie and J. Du, *J. Phys. Chem. C*, 2011, **115**, 7596–7602.

92 E. Garnett and P. Yang, *Nano Lett.*, 2010, **10**, 1082–1087.

93 S. M. Wallace, W. Jeyaswan and N. Fukata, *Sol. Energy*, 2021, **224**, 666–671.

94 G. Fan, H. Zhu, K. Wang, J. Wei, X. Li, Q. Shu, N. Guo and D. Wu, *ACS Appl. Mater. Interfaces*, 2011, **3**, 721–725.

95 C. Xie, X. Zhang, K. Ruan, Z. Shao, S. S. Dhaliwal, L. Wang, Q. Zhang, X. Zhang and J. Jie, *J. Mater. Chem. A*, 2013, **1**, 15348–15354.

96 H. K. Raut, V. A. Ganesh, A. S. Nair and S. Ramakrishna, *Energy Environ. Sci.*, 2011, **4**, 3779–3804.

97 E. Shi, H. Li, L. Yang, L. Zhang, Z. Li, P. Li, Y. Shang, S. Wu, X. Li, J. Wei, K. Wang, H. Zhu, D. Wu, Y. Fang and A. Cao, *Nano Lett.*, 2013, **13**, 1776–1781.

98 X. Gan, R. Lv, H. Zhu, L. P. Ma, X. Wang, Z. Zhang, Z. H. Huang, H. Zhu, W. Ren, M. Terrones and F. Kang, *J. Mater. Chem. A*, 2016, **4**, 13795–13802.

99 K. Ding, X. Zhang, L. Ning, Z. Shao, P. Xiao and A. Hobailie, *Nano Energy*, 2018, **46**, 257–265.

100 K. Ding, X. Zhang, L. Ning, Z. Shao, P. Xiao, A. Ho-Baillie, X. Zhang and J. Jie, *Nano Energy*, 2018, **46**, 257–265.

101 Y. Tsuboi, F. Wang, D. Kozawa, K. Funahashi, S. Mouri, Y. Miyauchi, T. Takenobu and K. Matsuda, *Nanoscale*, 2015, **7**, 14476–14482.

102 J. H. Meng, X. Liu, X. W. Zhang, Y. Zhang, H. L. Wang, Z. G. Yin, Y. Z. Zhang, H. Liu, J. B. You and H. Yan, *Nano Energy*, 2016, **28**, 44–50.

103 M. J. Im, S. K. Hyeong, M. Park, S. K. Lee, T. W. Kim, G. Y. Jung and S. Bae, *ACS Omega*, 2021, **6**, 3973–3979.

104 C. W. Jang, D. H. Shin, J. S. Ko and S. H. Choi, *Appl. Surf. Sci.*, 2020, **532**, 147460.

105 C. Geng, X. Chen, S. Li, Z. Ding, W. Ma, J. Qiu, Q. Wang, C. Yan and H. J. Fan, *Energy Mater. Adv.*, 2021, **2021**, 8481915.

106 Y. Wu, X. Zhang, J. Jie, C. Xie, X. Zhang, B. Sun, Y. Wang and P. Gao, *J. Phys. Chem. C*, 2013, **117**, 11968–11976.

107 S. Kaulgud, R. Sharma, L. Jolly and B. K. Mishra, *Int. J. Inf. Technol.*, 2021, **13**, 1323–1330.

108 C. W. Jang, D. H. Shin and S. H. Choi, *J. Alloys Compd.*, 2021, **877**, 160311.

109 H. A. Chaliyawala, S. Vemuri, K. Lellala and I. Mukhopadhyay, *Mater. Today Proc.*, 2021, **45**, 3789–3794.

110 X. Zhang, C. Xie, J. Jie, X. Zhang, Y. Wu and W. Zhang, *J. Mater. Chem. A*, 2013, **1**, 6593–6601.

111 A. B. Sieval, C. L. Huisman, A. Schönecker, F. M. Schuurmans, A. S. H. Van der Heide, A. Goossens, W. C. Sinke, H. Zuilhof and E. J. R. Sudhölter, *J. Phys. Chem. C*, 2003, **107**, 6846–6852.

112 S. Maldonado, D. Knapp and N. S. Lewis, *J. Am. Chem. Soc.*, 2008, **130**, 3300–3301.

113 F. Zhang, B. Sun, T. Song, X. Zhu and S. Lee, *Chem. Mater.*, 2011, **23**, 2084–2090.

114 C. Xie, X. Zhang, Y. Wu, X. Zhang, X. Zhang, Y. Wang, W. Zhang, P. Gao, Y. Han and J. Jie, *J. Mater. Chem. A*, 2013, **1**, 8567–8574.

115 M. A. Rehman, I. Akhtar, W. Choi, K. Akbar, A. Farooq, S. Hussain, M. A. Shehzad, S. H. Chun, J. Jung and Y. Seo, *Carbon*, 2018, **132**, 157–164.

116 A. Alnuaimi, I. Almansouri, I. Saadat and A. Nayfeh, *Sol. Energy*, 2018, **164**, 174–179.

117 J. Schmidt, A. Merkle, R. Brendel, B. Hoex, M. C. M. Van De Sanden and W. M. M. Kessels, *Prog. Photovoltaics*, 2008, **16**, 461–466.

118 I. Matacena, P. Guerriero, L. Lancellotti, E. Bobeico, N. Lisi, R. Chierchia, P. D. Veneri and S. Daliento, *IEEE Trans. Electron Devices*, 2023, **70**, 4243–4250.

119 J. M. Kim, S. W. Seo, D. H. Shin, H. S. Lee, J. H. Kim, C. W. Jang, S. Kim and S. H. Choi, *Curr. Appl. Phys.*, 2017, **17**, 1136–1141.

120 V. Ferguson, S. R. P. Silva and W. Zhang, *Energy Environ. Mater.*, 2019, **2**, 107–118.



121 C. W. Jang, J. M. Kim and S. H. Choi, *J. Alloys Compd.*, 2019, **775**, 905–911.

122 P. Liu, J. Liu, B. Zhang, W. Zong, S. Xu, Y. Liu and S. Cao, *J. Mater. Sci.*, 2019, **54**, 12688–12697.

123 M. Chen, Y. Wang, W. Ma, Y. Huang and Z. Zhao, *ACS Appl. Mater. Interfaces*, 2020, **12**, 28510–28519.

124 K. Cui, A. S. Anisimov, T. Chiba, S. Fujii, H. Kataura, A. G. Nasibulin, S. Chiashi, E. I. Kauppinen and S. Maruyama, *J. Mater. Chem. A*, 2014, **2**, 11311–11318.

125 M. Zhong, D. Xu, X. Yu, K. Huang, X. Liu, Y. Qu, Y. Xu and D. Yang, *Nano Energy*, 2016, **28**, 12–18.

126 L. Yang, X. Yu, M. Xu, H. Chen and D. Yang, *J. Mater. Chem. A*, 2014, **2**, 16877–16883.

127 C. Xie, X. Zhang, Y. Wu, X. Zhang, X. Zhang, Y. Wang, W. Zhang, P. Gao, Y. Han and J. Jie, *J. Mater. Chem. A*, 2013, **1**, 8567–8574.

128 A. Suhail, G. Pan, D. Jenkins and K. Islam, *Carbon*, 2018, **129**, 520–526.

129 X. Liang, B. A. Sperling, I. Calizo, G. Cheng, C. A. Hacker, Q. Zhang, Y. Obeng, K. Yan, H. Peng, Q. Li, X. Zhu, H. Yuan, A. R. Hight Walker, Z. Liu, L. M. Peng and C. A. Richter, *ACS Nano*, 2011, **5**, 9144–9153.

130 M. Her, R. Beams and L. Novotny, *Phys. Lett. A*, 2013, **377**, 1455–1458.

131 M. F. Bhopal, K. Akbar, M. A. Rehman, D. Won Lee, A. ur Rehman, Y. Seo, S. H. Chun and S. H. Lee, *Carbon*, 2017, **125**, 56–62.

132 D. Xu, X. Yu, L. Yang and D. Yang, *Superlattices Microstruct.*, 2016, **99**, 3–12.

133 M. Ye, Z. Zhang, Y. Zhao and L. Qu, *Joule*, 2018, **2**, 245–268.

134 W. S. Yang, B. W. Park, E. H. Jung, N. J. Jeon, Y. C. Kim, D. U. Lee, S. S. Shin, J. Seo, E. K. Kim, J. H. Noh and S. IlSeok, *Science*, 2017, **356**, 1376–1379.

